Separation of methane and hydrogen in a 3D-printed porous carbon monolith

Matheus Raphael Diniz Junqueira

Dissertation presented to the School of Technology and Management of Bragança to obtain the Master Degree in Chemical Engineering. Work developed under the Dual Degree Program between the Polytechnic Institute of Bragança (IPB) and the Federal Center for Technological Education of Minas Gerais (CEFET-MG).

Work oriented by:

Prof. PhD José A. C. Silva

Prof. PhD Marcello Rosa Dumont

Bragança

2025

Acknowledgement

Firstly, I would like to express my sincere gratitude to the team at the CIMO laboratory, especially to Adriano, for his invaluable assistance throughout the experiments, helping me overcome challenges and clarify doubts, which significantly improved my results. I am also grateful to Ezzeldin for introducing me to the experiments. Their support, patience, and hospitality made me feel welcomed and comfortable, while also giving me the opportunity to make new friends.

I would also like to acknowledge my supervisor, Professor José Silva, for the opportunity to conduct this research. Even though I was new to the institution, I was treated with respect and given the support I needed to develop. I would also like to thank Professor Marcello Dumont, my advisor at CEFET-MG, who had already advised me during my final course work and assisted me choose a thesis topic that was more closely aligned with the field of Materials Engineering. I would like to thank Center for Technological Education of Minas Gerais (CEFET-MG) and Polytechnic Institute of Bragança (IPB) for the opportunity to carry out this work of double degree program in Portugal and experience an incredible year on the other side of the Atlantic Ocean.

I would also like to thank Adriano S. Silva for synthesising the 3D-printed carbon-based monolith during his stay at the *Technische Universität Darmstadt* (Germany) under the supervision of Professor Bastian Etzold. This work results from joint financial support from FCT (Portugal) and DAAD (Germany)

In addition, I would like to thank my family for their constant support during the double degree process, for the calls that made me miss them, and for the life updates. To my friends in Belo Horizonte, who encouraged me and always believed in my success

abroad, I am deeply grateful. Their shared memories remind me that distance isn't so bad and that we'll soon be together again. To the friends I've made here, especially the residents of Zamora 10, thank you for your support, for teaching me to use new tools, for the unexpected cakes, and for the relaxed conversations that made living together more enjoyable. And to Arielle, for being by my side throughout this journey, offering support and partnership during all the challenges we faced, my deepest gratitude and affection.

Abstract

The efficient separation of methane (CH_4) and hydrogen (H_2) is a key challenge in industrial processes such as steam methane reforming (SMR), which is the primary technology used for hydrogen production; however, the generated gas contains impurities such as carbon monoxide (CO), carbon dioxide (CO_2), and unreacted methane, which must be removed to ensure high-purity H_2. The separation of these gases is commonly performed through pressure swing adsorption (PSA) using adsorbent materials such as zeolites (e.g., zeolite 13X) and activated carbons. However, these adsorbents often present challenges, including high pressure drop and limited control over pore structure.

In this context, this study investigates a 3D-printed porous carbon monolith with tetragonal cubic centred unit cells, designed to maximize CH_4 selectivity over H_2 while reducing pressure drop due to its highly controllable structural design. The material was characterized using fixed-bed adsorption experiments analyzed via flow gas chromatography, including single-component (H_2 and CH_4) and binary adsorption (CH_4/H_2 mixtures) at 303 K, 313 K, and 343 K, with pressures up to 30 bar. Adsorption equilibrium modelling was conducted using the Dual-Site Langmuir (DSL) isotherm, accurately describing the gas-monolith interactions.

Results showed that H_2 adsorption was negligible under all tested conditions. For CH_4, the maximum adsorption experimental capacity was 3.25 $mol.kg^{-1}$ at 303 K and 30 bar. Equilibrium isotherms confirmed material heterogeneity, with two distinct adsorption sites, each with its own adsorption capacity. The isosteric heat of adsorption ranged from 17.5 to 17.1 $kJ.mol^{-1}$, indicating a moderate physisorption mechanism. In binary adsorption experiments at 303 K and 5 bar, CH_4 adsorption reached 2.10 $mol.kg^{-1}$ for

an experimental 76/24 (% vol.) CH_4/H_2 mixture, reinforcing the material's selectivity, closely matching the values predicted by the isotherm from single component experiments.

These findings highlight the potential of 3D-printed porous carbon monoliths for selective CH_4 separation in PSA processes applied to SMR, offering a promising alternative with lower pressure drop and greater structural control compared to conventional adsorbents.

Keywords: 3D printing, porous carbon monolith, methane, hydrogen, adsorption isotherms, gas separation, adsorption, flow gas chromatography.

Resumo

A separação eficiente de metano (CH_4) e hidrogênio (H_2) é um desafio fundamental em processos industriais, como a reforma do metano a vapor (SMR), que é a principal tecnologia utilizada para a produção de hidrogênio. No entanto, o gás gerado contém impurezas, como monóxido de carbono (CO), dióxido de carbono (CO_2) e metano não reagido, que devem ser removidas para garantir um H_2 de alta pureza. A separação desses gases é geralmente realizada por adsorção com oscilação de pressão (PSA), utilizando materiais adsorventes como zeólitos (por exemplo, zeólito 13X) e carvões ativados. No entanto, esses adsorventes frequentemente apresentam desafios, incluindo elevada queda de pressão e controle limitado sobre a estrutura porosa.

Neste contexto, este estudo investiga um monólito de carbono poroso impresso em 3D com células unitárias cúbicas tetragonais centradas, projetado para maximizar a seletividade do CH_4 sobre o H_2, ao mesmo tempo que reduz a queda de pressão devido ao seu design estrutural altamente controlável. O material foi caracterizado por meio de experimentos de adsorção em leito fixo, analisados por cromatografia gasosa de fluxo, incluindo adsorção de componente único (H_2 e CH_4) e adsorção binária (misturas CH_4/H_2), em temperaturas de 303 K, 313 K e 343 K e pressões de até 30 bar. A modelagem do equilíbrio de adsorção foi realizada utilizando a isoterma de Langmuir de sítio duplo (DSL), descrevendo com precisão as interações entre os gases e o monólito.

Os resultados mostraram que a adsorção de H_2 foi insignificante em todas as condições testadas. Para o CH_4, a capacidade máxima experimental de adsorção foi de 3.25 $mol.kg^{-1}$ a 303 K e 30 bar. As isotermas de equilíbrio confirmaram a heterogeneidade do material, com dois sítios de adsorção distintos, cada um com a sua própria capacidade de

adsorção. O calor isostérico de adsorção variou entre 17.5 e 17.1 $kJ.mol^{-1}$, indicando um mecanismo de fisisorção moderada. Nos experimentos de adsorção binária a 303 K e 5 bar, a adsorção de CH_4 atingiu 2.10 $mol.kg^{-1}$ para uma mistura experimental de 76/24 (% vol.) CH_4/H_2, reforçando a seletividade do material e apresentando valores próximos aos previstos pela isoterma nos experimentos de componente único.

Essas descobertas destacam o potencial dos monólitos de carbono poroso impressos em 3D para a separação seletiva de CH_4 em processos de PSA aplicados ao SMR, oferecendo uma alternativa promissora com menor queda de pressão e maior controle estrutural em comparação com adsorventes convencionais.

Palavras-chave: Impressão 3D, monólito de carbono poroso, metano, hidrogênio, isotermas de adsorção, separação de gases, adsorção, cromatografia gasosa de fluxo.

Contents

List of Tables

List of Figures

List of Symbols

Acronyms

3D Three-dimensional

AC Activated Carbon

APC Advanced Pneumatic Control

ASTM American Society for Testing and Materials

BAPO Phenylbis(2,4,6-trimethylbenzoyl)phosphine oxide

BPC Back pressure controller

CAD Computer-aided design

CMS Carbon molecular sieves

DLP Digital Light Processing

DMLS Direct metal laser sintering

DOctP Bis(2-ethylhexyl) phthalate

DSL Dual-site Langmuir

DSS Dual-site Sips

DVB Divinylbenzene

EBM Electron Beam Melting

FDM Fused deposition modeling

FGD Flue gas desulfurization

GCMC Grand canonical Monte Carlo

GH Green Hydrogen

ILs Ionic liquids

LENS Laser Engineered Net Shaping

LOM Laminated Object Manufacturing

MFC Mass flow controller

MOFs Metal-organic frameworks

PETA Pentaerythritol tetraacrylate

POPs Porous organic polymers

PSA Pressure swing adsorption

SHS Selective Heat Sintering

SLA Stereolithography

SLS Selective laser sintering

SMR Steam Methane Reforming

TCD Thermal conductivity detector

TSA Temperature Swing Adsorption

UAM Ultrasonic Additive Manufacturing

UV Ultra violet

Nomenclature

b Adsorption affinity constant of adsorbate species, (bar^{-1})

b_∞ Adsorption affinity constant of adsorbate species at infinity temperature, (bar^{-1})

C_f Concentration of the adsorbate species in the feed, $(mol.m^{-3})$

F Molar flow rate of adsorbate species, $(mol.s^{-1})$

F_f Molar flow rate of adsorbate species in the feed, $(mol.s^{-1})$

m_{ads} Mass of adsorbent (kg)

N Number of data points (experimental loadings)

n Heterogenity index of component, (-)

n_0 Heterogenity index of component at reference temperature, (-)

p Partial pressure of adsorbate species, (bar)

q_{exp} Adsorption loading (experimental) $(mol.kg^{-1})$

q_m Adsorption loading (given by the isotherm model) $(mol.kg^{-1})$

q_{sat} Saturation loading capacity $(mol.kg^{-1})$

R Universal gas constant $(J.mol^{-1}.K^{-1})$

T Temperature, (K)

t Time, (s)

T_0 Reference temperature, (K)

t_s Saturation time, (s)

V_{ac} Volume of adsorption column, (m^3)

y Molar fraction of adsorbate species, (-)

y_f Molar fraction of adsorbate species in the feed, (-)

Subscripts

1 Site 1

2 Site 2

∞ Infinity condition

ac Adsorption column

ads Adsorbent

exp Experimental

f Feed

m Model

s Saturation time

sat Saturation

st Isosteric

Greek Letters

α Constant parameter (heterogeneity index - Sips isotherm), (-)

ΔH Heat of adsorption of adsorbate species, ($J.mol^{-1}$)

ΔH_{st} Isosteric heat of adsorption of adsorbate species, ($J.mol^{-1}$)

$\Delta \overline{q}$ Mean relative deviation between experimental loading and isotherm model, (-)

ε_b Bed porosity (-)

Chapter 1

Introduction

1.1 Motivation

The growing global demand for sustainable energy and the imperative to reduce greenhouse gas emissions have accelerated research in gas separation technologies. Among these gases, methane (CH_4) and hydrogen (H_2) stand out: hydrogen plays a critical role as an energy carrier in renewable systems, while methane, a major component of natural gas, serves as a potential hydrogen source through reforming processes. In steam methane reforming (SMR), CH_4 reacts with steam in the presence of a catalyst to produce hydrogen, making it a crucial feedstock for large-scale hydrogen production. However, the effective and efficient separation of CH_4 and H_2 remains a key challenge in improving both energy efficiency and environmental sustainability [1–3].

Current gas separation technologies, including cryogenic processes, membranes, and adsorption on porous materials, each present specific drawbacks. While cryogenic processes and membranes offer good selectivity, they are often expensive and energy-intensive. Adsorption using porous materials, such as zeolites and activated carbons, offers a promising alternative due to its potential low cost and efficiency. However, these materials face challenges in achieving precise control over structural properties, leading to inconsistent

performance. As reviewed by Amin *et al.* (2023) [4] these limitations in hydrogen separation technologies, such as low recovery rates and high costs, highlight the need for innovative solutions.

The innovation of this study lies in the use of a Three-dimensional (3D)-printed porous carbon monolith for the efficient separation of CH_4 and H_2. Unlike traditional adsorbents, which are typically used in the form of pellets or beads, this monolith is fabricated as a structured 3D material, providing a significant advantage in reducing pressure drop, which is a critical factor in adsorption-based separation processes. Traditional separation technologies face significant economic and operational challenges, especially in low hydrogen concentration mixtures.

In addition, 3D printing enables the fabrication of porous materials with controlled geometry and customizable properties, allowing precise optimization of structural features such as pore size distribution. This level of control not only enhances selective adsorption and improves separation efficiency but also mitigates pressure losses, leading to more energy-efficient operation. Therefore, this study presents a potentially scalable and cost-effective solution, addressing the limitations of existing technologies such as pressure swing adsorption (PSA), which struggles with low hydrogen concentrations and requires large units to handle diluted gas mixtures.

1.2 Objectives of the Study

The general objective of this thesis is to study the capacity of a 3D-printed carbon monolith for the efficient separation of CH_4 and H_2. Specifically, the study seeks to:

1. Evaluate the adsorption efficiency of these materials by a flow gas chromatography method under certain operational conditions, such as pressure (1 to 30 bar) and temperature (303 K, 313 K and 343 K), to analyze their performance for gas separation of different mixtures levels of CH_4 and H_2.

2. Determine equilibrium constants, such as adsorption affinity, adsorption enthalpy,

and the loading capacity of CH_4 and H_2 in the 3D printed-Activated Carbon (AC) monolith studied.

1.3 Structure of the Thesis

The remaining portion of this thesis is structured into four main chapters, each focusing on a specific aspect of the research:

- Chapter 2: State of Art and Study of Tools

  This chapter provides a detailed literature review on 3D printing techniques, their applications in chemical engineering, and the structural characteristics of porous materials used for gas adsorption. It highlights the current advancements, challenges, and limitations in methane and hydrogen separation processes.

- Chapter 3: Fixed Bed Adsorption: Experimental and Modelling

  The chapter describes the experimental setup and procedures, focusing on the fabrication of 3D-printed monolith and the breakthrough experimental apparatus used to measure adsorption equilibrium data of CH_4 and H_2. It also explains the operational conditions under which the gas separation experiments were conducted.

- Chapter 4: Results and Discussion

  This chapter presents the experimental data of CH_4 and H_2 collected on the selected 3D printed monolith. It includes also a comparison of the collected data with other different types of adsorbents and a discussion on the equilibrium and performance of the binary CH_4/H_2 adsorption. It also provides some insights into adsorption isotherm results.

- Chapter 5: Conclusion and Future Work

  This chapter summarizes the key findings of the research, discusses their implications, and suggests potential directions for future studies, especially regarding improvements in the 3D-printed monolith and its potential application in industrial gas separation processes.

Chapter 2

State of Art and Study of Tools

2.1 3D Printing Techniques

2.1.1 History and Evolution

Three-dimensional (3D) printing technology, also known as additive manufacturing, has its origins in the layer-by-layer fabrication of three-dimensional structures directly from Computer-aided design (CAD) models. The first significant advancement in 3D printing occurred in 1980 with the creation of the Stereolithography (SLA) process by Charles Hull, which led to its introduction as a commercial product. This method involves the creation of 3D objects in a layer-by-layer process utilising a photosensitive resin that hardens when exposed to ultraviolet light [5].

Following this initial development, 3D printing technology evolved rapidly, with the introduction of various other techniques such as Fused deposition modeling (FDM), Selective laser sintering (SLS), Direct metal laser sintering (DMLS). These advancements expanded the range of materials that could be used, including thermoplastics, metals, ceramics, and more recently, food and biological materials [6].

As the technology advanced, 3D printing transitioned from being primarily utilized as a prototyping tool to being employed in mass production across a diversifying range of industries. It has been employed in a number of different sectors, including aerospace,

automotive, healthcare and fashion. This evolution has resulted in the emergence of new possibilities for customization, the reduction of waste, and an increase in production efficiency [7]. In chemical engineering, these techniques offer new possibilities for designing highly customizable materials, particularly porous carbon structures, which are promising for gas adsorption and separation processes.

Over the last decade, 3D printing has continued to demonstrate remarkable versatility and application, making significant impacts on sectors such as healthcare, where it is used to create custom prosthesis and implants, and aerospace, where it is used to manufacture lightweight components. The technology is still expanding, with ongoing research into new materials and methods that promise to further extend its capabilities [8].

An overview describing the techniques, applications, and materials used in 3D printing [9] mention that according to American Society for Testing and Materials (ASTM) F2792 [10], the technologies around 3D printing are catalogued into seven groups, including the sheet lamination, vat photopolymerization, directed energy deposition, material extrusion, material jetting, powder bed fusion and binding jetting. For each of these technologies there are targeted applications, so there is no debate about which machine is better then other.

- **Sheet Lamination**: This 3D printing process involves bonding sheets of material to create parts. Technologies like Laminated Object Manufacturing (LOM) and Ultrasonic Additive Manufacturing (UAM) use this method. Benefits include the ability to produce full-colour prints, lower costs, easy material handling, and capacity for recycling. LOM is noted for producing complex geometries at a lower cost, while UAM uses sound to bond metal layers [11].

- **Vat Photopolymerization**: A common 3D printing technique that cures photoreactive polymers using lasers, light, or UV rays. Examples include Stereolithography (SLA) and Digital Light Processing (DLP). SLA depends on photo initiators and UV conditions, while DLP uses an arc lamp and is faster due to applying light to the entire surface at once. This method is known for producing high-quality,

detailed products [12].

- **Directed Energy Deposition**: A complex 3D printing process used to repair or add material to existing parts. It offers high control over grain structure and is typically used with metals. This method includes technologies like laser deposition and Laser Engineered Net Shaping (LENS), which are suitable for industries like aerospace and oil and gas due to their scalability and versatility [13].

- **Material Extrusion**: A widely used, low-cost 3D printing method that can print multi-material and multi-color objects. Fused Deposition Modelling (FDM) is a primary example, using heated thermoplastic filament to build parts layer by layer. FDM can produce fully functional parts and is used in applications like creating 3D bone models [14].

- **Material Jetting**: This process involves selectively depositing droplets of photosensitive material that solidifies under UV light to build parts layer by layer. It offers high dimensional accuracy, smooth surface finishes, and supports multi-material printing, including polymers and ceramics [6].

- **Powder Bed Fusion**: This process includes techniques like Electron Beam Melting (EBM), Selective Laser Sintering (SLS), and Selective Heat Sintering (SHS). It uses lasers or electron beams to fuse powder materials such as metals, ceramics, and polymers. SLS, developed in 1987, is noted for its speed, accuracy, and versatility in creating metal, plastic, and ceramic objects [15].

- **Binder Jetting**: A 3D printing process where a liquid binder is deposited onto a powder bed to join particles. It is fast, simple, and cost-effective, capable of producing large objects from a variety of materials, including metals and ceramics. Binder jetting is often used for producing casting patterns and large-volume products from sand [16].

2.1.2 Applications in Chemical Engineering

There is a significant potential for 3D printing to improve chemical engineering processes and components, particularly for separations related to energy production and greenhouse gas emission control. There are examples where 3D printing could be used to produce components and devices with improved efficiency in gas absorption with liquid solvents. Adsorption processes are already used for a variety of gas treatment applications, including natural gas sweetening, flue gas desulfurization (FGD), and the emerging applications of pre- and post-combustion carbon dioxide capture. Furthermore, Bara *et al.* (2015) [17] illustrate their proof-of-concept work to date in applying this technology to the design, fabrication, and investigation of novel and improved devices and components for gas absorption processes.

Current advances in chemical engineering are often linked to the concept of process intensification, which aims to produce chemical products in a more sustainable and efficient way [18]. One focus is the introduction of innovative principles in plant design that lead to improvements in process efficiency. It is believed that the main opportunities for process intensification through additive manufacturing are in continuous flow reactions that use heterogeneous catalysts and are currently limited by mass, momentum, or energy transfer.

However, more complex scenarios such as non-isothermal reactions or catalysts and reactors dealing with multiphase flows are also likely to prove valuable. After introducing a number of relevant additive fabrication tools, the potential of these technologies is illustrated by selected recent achievements and suggested future directions [19].

Amores *et al.* (2022 [20] indicates that in chemical engineering, the primary objective of obtaining complex or intricate shapes is to increase surface area. 3D printing enables the fabrication of reactors, mixing devices, and packed columns with geometries that enhance performance in both continuous flow and batch processes [19, 21–25]. Additionally, filters (Xu *et al.*, [26]), adsorbent structures (Mendes *et al.*, [27]) and membranes (Issac and Kandasubramanian, [28]; Tijing *et al.*, [29]) can be 3D printed, which can

be highly beneficial in environmental applications. In this regard, the characteristics of 3D printing can facilitate the development of more sustainable chemical production systems. These technologies typically involve a reduced use of raw materials and facilitate reuse (Nadagouda *et al.*, [30]). In contrast, they offer a means of bringing manufacturing closer to the point of sale or use, with the design being the only component that travels, rather than the product and/or its components. This reduces the environmental impact associated with transport.

2.2 Porous Materials

Over the past few decades, both industry and the scientific community have focused on carbon capture and storage and carbon capture and utilization as part of the mitigation program. The key to achieving their goals is to capture CO_2 selectively from the gas mixture [31–37]. There are several technologies to capture CO_2, including chemical absorption, membrane separation, adsorption and cryogenic CO_2 capture. The traditional method of absorption by liquid amines, and some self-proclaimed green solvents, including task-specific ionic liquids (ILs), amino acid-functionalized ILs, IL-mixed solvents, and deep eutectic solvents, prove to be very conventional and are proposed as promising materials [38]. However, despite their advantages, they suffer from serious corrosion problems, significant energy loss, high sorbent cost, lower gas-liquid interfacial area, and ineffective regeneration [39]. Due to these limitations, CO_2 adsorption by solid porous material has advantages such as high uptake efficiency, easy regeneration and high adsorption capacity under humid conditions, easy handling and material stability.

Currently, a wide variety of solid adsorbents have been used for CO_2 capture, including metal-organic frameworks (MOFs), zeolites, mesoporous silica, clay, porous carbons, porous organic polymers (POPs), hydrotalcite, organic-inorganic hybrids and metal oxides. These solid porous materials have different physicochemical interactions with CO_2 molecules [40].

- **Metal-organic frameworks** are a class of crystalline, porous materials composed

of inorganic ions or clusters linked by multitopic organic ligands [41, 42]. A high degree of control over pore size, shape, and surface chemistry can be achieved by pre- or post-synthetic modification. The development of metal-organic frameworks for CO_2 capture applications has largely focused on the use of charge-dense adsorption sites, such as coordinatively unsaturated metal cations, to select for CO_2. However, as with cationic binding sites in zeolites, these adsorption sites are prone to water passivation in carbon capture applications involving humid process or emission streams [43, 44]. Accordingly, frameworks with CO_2-binding functionalities, such as amines, have gained increasing attention in recent years. Alternatively, stable and scalable frameworks that retain partial CO_2 capacity after water adsorption may offer a rapid route to commercialisation. Functionalization with hydrophobic groups can also improve capture performance from humid streams [45, 46].

- **Zeolites** have also reached a state of maturity for industrial separations. The commercialisation of these aluminosilicate materials has been facilitated by their high stability, a result of the strong tetrahedral Al-O and Si-O bonds in their constituents. This stability has in turn facilitated the processing of zeolites into industrially viable structured forms, such as pellets. In addition, the crystalline nature of zeolites has enabled computational screening of known and predicted structures to identify optimal architectures for specific separations [46].

- As with amine solutions, **polyamine-functionalised silicas** exploit the selective acid-base chemistry of amines to enable effective CO_2 capture from humid streams. By using a solid support rather than an aqueous solvent medium, the energy costs associated with heating the solvent can be avoided, potentially enabling more efficient capture processes. Polyamines can be physically impregnated (class 1) or covalently grafted (class 2) onto the silica support and selectivity is achieved by the formation of ammonium carbamate, carbamic acid or bicarbonate species, with product distribution varying as a function of amine identity, proximity of amine to adjacent amine groups and water content [46].

- **Clay** is a common term used to refer to a specific clay mineral or a mixture of single or multiple clay minerals, including small amounts of organic matter and metal oxides. Clays are hydrated aluminium phyllosilicates formed naturally by hydrothermal alteration of rocks. Many studies have investigated the clay-based materials as one of the effective adsorbents for CO_2 capture, including kaolinite, halloysite, bentonite, smectite, montmorillonite or sepiolite as starting materials. Clay minerals are not susceptible to chemical modification, textural properties can be enhanced and microporosity can be improved [40].

- **Porous carbon-based adsorbents** are increasingly being investigated as a potential solution for CO_2 capture. They offer a number of advantageous properties, including high accessibility, physiochemical stability, affordability, and the ability to modify their porosity, which makes them an attractive option for this application. Granular and powder-activated carbons represent the conventional carbon adsorbents. New types of carbon are also employed as potential sorbents, including fabrics, activated carbon fibres and felts, which can be synthesised using different types of precursors, including coal, rayon, petroleum pitch and viscose. Activated carbons for CO_2 adsorption are manufactured through the carbonization and subsequent physical or chemical activation of a diverse range of natural sources, including biomass, glucose, and plant-based materials, as well as synthetic precursors such as triazine-based persistent organic pollutants (POPs) and petroleum pitch. The classification of activated carbons is based on their surface characteristics and preparation technique. The most common types are powdered activated carbon, granulated activated carbon, spherical activated carbon, impregnated carbon, and polymer-coated carbon [40].

2.2.1 Carbon Monoliths

Currently, most research works deal with the application of 3D printed monoliths as adsorbents for CO_2 capture from air/enclosed environments or post-combustion flue gas.

As observed by Henrique *et al.* (2023) [47], the recurrent issues encountered when utilising these shaped materials in packed bed systems, particularly when higher through puts are desired, impose constraints on the operation of such processes at optimal energy consumption and overall system efficiency. The disadvantages of this approach include the considerable pressure drop that occurs at high gas velocities, restrictions on mass transfer due to the diffusion of gas into and out of the adsorbents, and low mechanical and attrition resistance. It may be possible to enhance the mass transfer characteristics of monoliths by employing structures with reduced channel width and wall thickness or a more optimal shape.

Thakkar *et al.* (2016) [48] discusses a notable effort to develop new strategies for producing structured adsorbents in alternative configurations that could address the limitations of traditional packing systems. In this regard, monolithic engineered geometry has emerged as a prominent alternative for the manufacture of adsorbent materials. Monolithic contactors present a distinctive geometry configuration comprising parallel channels (i.e., a continuous body with identical channels), which do not impede fluid flow. Consequently, this results in a uniform flow pattern with a lower pressure drop across the bed, while also offering enhanced mass and heat transfer characteristics. Such well-designed, robust contactors are structured materials in which the shape and diameter of the parallel channels, the wall thickness, and their cell density are controllable.

2.2.2 Types of Carbons Monoliths

Lozano-Castelló *et al.* (2002) [49] demonstrates the effect of the type of binder on the monolith properties. In his study, is shown some different types of binders: a humic acid-derived sodium salt (HAS) from Acros organics, polyvinyl alcohol (PVA), a novolac phenolic resin (PR) (Georgia Pacif 5506), a proprietary binder from Waterlink Sutcliffe Carbons (WSC), Teflon (TF) from Du Point and a adhesive cellulose-based binder (ADH) (Saint Honoré).

- **Humic Acid-Derived Sodium Salt (HAS)**: This binder is derived from humic

acids, which are complex organic substances found in soil. They are known for their adsorption properties and ability to form complexes with metals [50].

- **Polyvinyl Alcohol (PVA)**: PVA is a water-soluble synthetic polymer often used as a binder due to its excellent adhesion and film-forming properties. It is known to enhance the mechanical strength and thermal stability of adsorbent materials [50].
- **Novolac Phenolic Resin (PR)**: This type of phenolic resin is used as a binder because of its high thermal and chemical resistance. Novolac resins are often utilized in applications requiring stability at high temperatures [51].
- **Proprietary Binder from Waterlink Sutcliffe Carbons (WSC)**: This is a proprietary binder, meaning its exact composition is not publicly disclosed. However, proprietary binders are generally formulated to optimize specific properties such as adsorption capacity and mechanical strength [52].
- **Teflon (TF)**: Teflon, or polytetrafluoroethylene (PTFE), is known for its non-stick properties and chemical resistance. As a binder, it can provide a low-friction surface and high resistance to chemicals.
- **Adhesive Cellulose-Based Binder (ADH)**: This binder is derived from cellulose, a natural polymer found in plants. Cellulose-based binders are valued for their biodegradability and natural adhesive properties.

2.3 Effect of Monoliths Structural Characteristics on CH_4 Adsorption

In the quest for efficient methane capture and storage, the structural characteristics of monolithic adsorbents play a pivotal role. Monoliths, with their unique combination of low pressure drop and high surface area, present significant advantages for gas adsorption processes. However, optimizing these structures for methane adsorption requires a deep understanding of their characteristics.

The monoliths studied by Liu *et al.* (2021) [53] are zeolite-carbon composites designed to enhance the efficiency of CH_4 and N_2 separation. The structure of these monoliths combines the adsorptive properties of zeolite with the robustness and thermal conductivity of carbon, providing an efficient platform for selective gas adsorption. The monoliths feature a high surface area and adjustable porous structure, which are critical for maximizing CH_4 adsorption capacity. By modifying the Si/Al ratio in zeolites and adjusting pore distribution, it is possible to control the selectivity and adsorption capacity, directly impacting the monoliths performance. The CH_4 adsorption behaviour of the monoliths is influenced by factors such as material density, pore size, and surface polarization. The presence of exchangeable cations, like Na^+ or Ca^{2+}, can alter the material's affinity for CH_4, improving selectivity in the presence of N_2.

As reported by Abubakar *et al.* (2024) [54], the effects of the structural characteristics of monoliths on CH_4 adsorption, as discussed in the document, revolve around the precision engineering of pore structures within activated carbon monoliths. These monoliths are manufactured using a three-dimensional printed sacrificial template method, which allows for the creation of highly controlled macro porous networks. Key structural characteristics that influence CH_4 adsorption include:

- **Interparticle Porosity**: The monoliths are designed with low interparticle porosity, ranging from 9 % to 24 %. This low porosity is crucial for maximizing the volumetric adsorption capacity of methane by reducing the amount of non-adsorbing space within the structure.

- **Macro Channel Network**: The use of 3D-printed templates enables the creation of macro channels with precise geometries and connectivity. These channels improve the mass transfer within the monolith, allowing for faster adsorption and desorption of methane, which is particularly beneficial for gas storage applications where rapid cycling is required.

- **Mechanical Integrity**: Despite the presence of macro channels, the monoliths exhibit excellent mechanical strength, withstanding forces up to 900 N before excessive

fracturing. This strength is essential for maintaining the structural integrity of the monoliths under operational pressures.

- **Customizable Structural Properties**: The monoliths structural properties, such as pore size distribution and channel geometry, can be finely tuned by adjusting the design of the 3D-printed templates. This customization allows the optimization of the monoliths for specific gas storage conditions, including those needed for efficient CH_4 adsorption.

These structural characteristics are integral to the monoliths performance in CH_4 adsorption, as they directly impact the efficiency, capacity, and durability of the gas storage system. The advanced fabrication technique ensures that these characteristics are precisely controlled, leading to enhanced gas storage capabilities.

The process of methane adsorption in carbon monoliths is a complex mechanism that is influenced by a range of structural and chemical factors. Carbon monoliths, distinguished by their interconnected porous networks and elevated surface areas, have emerged as a promising class of materials for gas storage and separation applications. In order to optimize the performance of these materials for methane adsorption, it is essential to gain an understanding of the key factors that influence this process and to be able to manipulate them. These include the surface area, pore size distribution, and pore volume, which directly impact the capacity and efficiency of methane adsorption. Additionally, the surface chemistry and the presence of functional groups on the carbon surface can significantly enhance the interaction between methane molecules and the monolith, resulting in improved adsorption performance [49].

Furthermore, the degree of the monoliths graphitization, macro porosity and overall structural integrity play a crucial role in determining the material's durability and functionality under operational conditions. The mechanical strength and thermal conductivity of the monolith ensure that it can tolerate the physical stresses and thermal cycles that are typical of industrial processes. In addition, factors such as density and the ability of the monolith to undergo regeneration without loss of adsorption capacity are crucial

for its practical application in cyclic processes. This chapter will explore these factors in detail, providing insights into how each contributes to the overall effectiveness of carbon monoliths in methane adsorption [54].

- The **porous texture** of carbon monoliths is a critical factor influencing their methane adsorption capacity. The adsorption of methane predominantly occurs in micropores (pores with diameters less than 2 nm, as defined by the IUPAC [55]), and thus the *micropore volume and size distribution* are directly related to the adsorption capacity of the material. The preparation of activated carbon monoliths frequently involves the utilization of diverse binders, which can impact the porous structure of the final monolith. For example, the use of certain binders may result in pore blockage, which in turn reduces the available micropore volume and consequently affects the methane adsorption capacity.

- The selection of an **appropriate binder** is also of great importance in the preparation of carbon monoliths. It is essential that binders possess specific properties to ensure that they do not excessively impede the micropore structure of the activated carbon. An effective binder should facilitate the formation of monoliths with favourable mechanical properties while minimising the obstruction of micropores. The impact of different binders, including polyvinyl alcohol, phenolic resin, and proprietary binders, on micropore volume and adsorption performance varies. For instance, studies have demonstrated that certain binders, such as phenolic resin, can result in substantial micropore blocking, whereas others, like a proprietary binder from Waterlink Sutcliffe Carbons (WSC), may exert a less pronounced influence on pore structure.

- The **density** of carbon monoliths is a critical parameter for methane storage. Higher density monoliths generally offer better packing efficiency, which is essential for maximizing the volumetric methane storage capacity. However, there is often a trade-off between density and micropore accessibility. While higher density monoliths reduce

interparticle voids and improve packing efficiency, they may also lead to reduced micropore accessibility if the binder contributes to significant pore blockage. Therefore, achieving an optimal balance between monolith density and micropore accessibility is key to enhancing methane adsorption performance.

- The **mechanical strength** of carbon monoliths is vital for their practical application in methane storage systems, especially under conditions of repeated pressurization and depressurization. Monoliths must possess sufficient mechanical strength to withstand these conditions without fracturing or degrading. The mechanical properties of monoliths are largely influenced by the binder used and the method of monolith preparation. For example, compression tests have shown that different binders contribute differently to the monolith's strength, with some providing a better balance between strength and adsorption capacity than others.

- The rate of methane adsorption in carbon monoliths is influenced by the **kinetics of gas diffusion** within the porous structure. Fast adsorption kinetics are desirable for efficient storage and retrieval of methane. The preparation conditions of carbon monoliths, including the choice of binder and the resultant pore structure, play a significant role in determining the kinetic behaviour. Preliminary studies suggest that well-prepared monoliths do not exhibit significant diffusional limitations, indicating that with proper binder selection and preparation techniques, the adsorption process can be optimized for rapid methane uptake.

2.4 Gas Adsorption Processes

Gas adsorption processes are very important in the separation and purification of gases, widely applied in industries ranging from environmental protection to chemical production. The fundamentals of these processes involve the adherence of gas molecules onto a solid surface, driven by various forces and interactions. This chapter delves into the principles, mechanisms, and key materials utilized in gas adsorption, providing an

understanding of how these processes work and their significance in industrial applications [56].Several experimental methods are employed to study gas adsorption, providing insights into the adsorption capacity and kinetics of the process.

The **volumetric method** involves expanding a gas from a pressure cell into an evacuated adsorption cell containing the adsorbent. The amount of gas adsorbed is determined by the change in pressure at equilibrium. This method is widely used for constructing adsorption isotherms.

As another method, there is the **gravimetric method** in which the weight change of the adsorbent due to gas adsorption is measured. This method provides a direct measurement of the adsorption capacity and is particularly useful for studying adsorption kinetics and diffusivity.

On this study, the chosen method used is a **flow gas chromatography method** technique to measure single and binary adsorption equilibrium isotherms.

2.4.1 CH_4 Adsorption Behaviour in Different Adsorbents Materials

2.4.1.1 Carbon-based Adsorbents

For activated carbon, there are studies that show their properties around the CH_4 adsorptions. Their are derived from the pyrolysis of carbon precursors, offers a compelling combination of stability, affordability, and versatility [46].

Also, activated carbon exhibits excellent adsorption and desorption capabilities, usually used for CO_2 adsorptions, rendering it particularly suitable for transportation applications that necessitate frequent recharging [57].

Especially, the CH_4/H_2 separation via adsorptive separation has become more crucial owing to the growing needs for the H_2 purification [58]. Typically, H_2 is generated through the CH_4 reforming process, introducing impurities like CO_2, CO, and CH_4 [59]. In order to purify H_2, these impurities must be effectively removed, with methane posing a significant challenge due to its similarity to hydrogen in chemical properties [60].

Previously, the research of Lozano-Castelló *et al.* (2002) [49] explored the agglomeration of high adsorption capacity powdered activated carbon for CH_4 storage using various binders. The majority of binders produced monoliths with good mechanical properties. However, they typically resulted in a reduction in adsorption capacity due to a decrease in activated carbon content and partial pore blocking, which was dependent on the binder type. The best adsorption performance was achieved with binders like PR, TF, ADH, and WSC, which minimally blocked micropores. Additionally, the study found no diffusional issues with methane adsorption in the monoliths.

Furthermore, Comroe *et al.* (2022) [61] successfully fabricated a 3D-printed carbon monolith using the direct ink method, marking the first synthesis of 3D-printed porous carbon along with poly(4-vinylphenol) and Pluronic F127 without a sacrificial template, achieving a good BET surface area of and a great total pore volume. As shown in Figure 2.1, adsorption studies demonstrated that the carbon monolith used had the highest selectivity for the CH_4/N_2 pair. Additionally, the carbon monolith demonstrated stable adsorption capacity and maintained its structure through repeated CO_2 loading and unloading cycles.

Moreover, the study of Park *et al.* (2024) [62] is focus on manipulate the pore structure of activated carbon by altering the composition of the carbon precursor to enhance CH_4 and H_2 storage and separation. By incorporating melamine as a sacrificial template and Cs^+ ions as activating agents, the micropore surface area and volume significantly increased, this study resulted in exceptional CH_4 and H_2 storage capacities. The materials also demonstrated a CH_4 good working capacity and moderate CH_4/H_2 selectivity.

2.4.1.2 Zeolites

Zeolites play a crucial role in the adsorption of methane due to their unique structure and properties as porosity, surface area and Si/Al ratio, which make them highly effective in separating CH_4 from other gases like nitrogen and carbon dioxide.

The study of Karimi *et al.* (2021) [63] on zeolite 4A focused on the adsorption isotherms

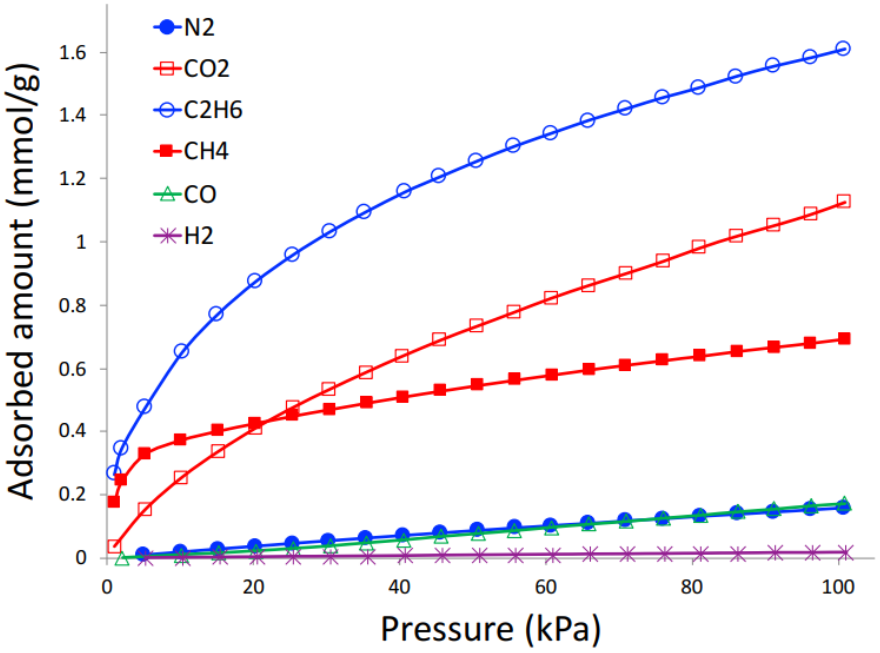

Figure 2.1: Gas adsorption isotherms on 3D printed porous carbon monoliths at 298 K.[61]

for gases such as CO_2, CH_4, and N_2 using binder-free beads, highlighting the material's efficiency in gas separation processes. For CH_4, the isotherms showed in the study demonstrated a typical Type I behaviour, indicating strong adsorption at lower pressures, followed by a plateau as saturation was approached. Zeolite 4A exhibited moderate adsorption capacity for CH_4 compared to CO_2, which displayed significantly higher adsorption due to its greater polarizability and affinity for the zeolite framework. These results underline the selective nature of zeolite 4A, making it suitable for gas separation applications such as removing CO_2 from methane-rich streams in natural gas processing and biogas upgrading.

The study of Streb and Mazzotti (2021) [64] on zeolite 13X presents adsorption isotherms for CH_4 and H_2 at various temperatures and pressures, showcasing the material's capacity to adsorb different gases. As described by Figure 2.2, the CH_4 isotherms exhibited a linear behaviour at low pressures, gradually approaching saturation as the

pressure increased to 30 bar. The findings highlighted that CH_4 has a moderate affinity toward zeolite 13X, characterized by an average isosteric heat of adsorption of -18.8 $kJ.mol^{-1}$. This value situates CH_4 adsorption capacity between the higher affinity of CO_2 and the significantly lower affinity of H_2. The study further validated the Sips isotherm model for CH_4 adsorption on zeolite 13X, confirming its reliability in describing single-component gas adsorption. Due to these characteristics, zeolite 13X is extensively utilized in the industry for applications such as natural gas purification, where it efficiently removes CO_2 and H_2O impurities, and in pressure swing adsorption (PSA) processes for gas separation, including the recovery of high-purity CH_4.

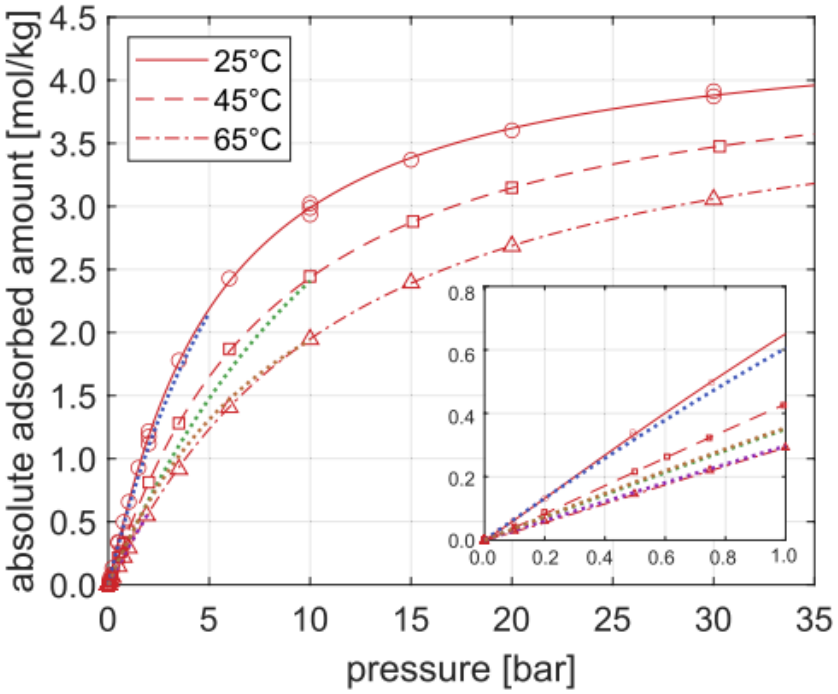

Figure 2.2: CH_4 adsorption isotherms on zeolite 13X. Lines indicate the fitted Sips isotherms. The low pressure region up to 1 bar is shown separately.[64]

2.4.1.3 Metal-organic Frameworks

The structure of MOFs forms a highly porous, cage-like framework with an enormous surface area, making it particularly attractive for applications in gas storage, separation,

and catalysis. The flexibility in the design of MOFs allows for the tuning of their properties, enabling the development of materials with specific characteristics tailored for various industrial applications, including the storage and separation of gases like methane (CH_4).

As another research, Li *et al.* (2022) [65] synthesized a series of ultra-microporous pillared MOFs, based on DMOF, through ligand and metal modulation to separate CH_4 and N_2 mixtures. Among them, DMOF-A2 demonstrated the highest CH_4 adsorption capacity (37 cm^3/g) and CH_4/N_2 selectivity (7.2). DMOF-A2 also showed good moisture resistance, with negligible water vapour uptake before 40 % relative humidity, minimizing humidity's impact on separation performance. The nonpolar aromatic rings in DMOF-A1, DMOF-A2, and DMOF-A3 enhanced separation by improving the pore environment and increasing hydrophobicity, protecting the metal-O bond from hydrolysis. Breakthrough experiments confirmed that DMOF-A2 effectively separates high-purity CH_4 from CH_4/N_2 mixtures, even under high humidity, making it an excellent material for CH_4/N_2 separation in moist conditions.

The study by Ullah *et al.* (2020) [66] investigated the methane (CH_4) adsorption performance of the metal-organic framework UMCM-1 at different temperatures and up to 1 bar pressure. The results showed that UMCM-1 has a CH_4 adsorption capacity of 0.45 $mmol.g^{-1}$ at 298.15 K, which is significantly lower than that of CO_2 (1.0732 $mmol.g^{-1}$). This difference was attributed to the weaker interactions of CH_4 with the porous framework due to its larger kinetic diameter and lower interaction forces. In addition, increasing the temperature resulted in an average decrease of 10.7 % in the adsorption capacity for both gases, highlighting the exothermic nature of the process. The study illustrated the Langmuir isotherm adsorption behaviour, further demonstrates the preferential adsorption of CO_2 by UMCM-1, demonstrating its potential as a promising candidate for selective gas separation.

Chapter 3

Fixed Bed Adsorption: Experimental and Modelling

Studying adsorbent materials means understanding their properties and performance under various conditions. Experimental techniques are crucial in characterizing these materials, providing insights into their surface area, pore structure, adsorption capacity and kinetics. These techniques optimize existing materials and aid in the discovery of new adsorbents for specific processes by measuring the adsorption of single and multicomponent gases for targeted processes.

In the context of fixed-bed adsorption processes, a gas or liquid stream is permitted to flow through a packed bed of adsorbent particles, where the adsorption of target molecules occurs. These processes are operated in a transient mode, meaning that the concentration of adsorbates in both the fluid and solid phases changes over time and position in the bed. A key characteristic of fixed-bed adsorption is the formation of breakthrough curves, which describe how the effluent concentration evolves over time. These curves are essential for evaluating adsorption efficiency, process scalability, and the measurement of the adsorption equilibrium and kinetic factors [67, 68].

This chapter will discuss the experimental and modelling aspects of fixed-bed adsorption, presenting the gas chromatography method as a fundamental technique for analyzing

gas-adsorbent interactions and measuring single and multicomponent isotherms fundamental for the design of adsorption processes. The breakthrough experimental apparatus is then introduced, covering the procedures for conducting adsorption experiments and measuring equilibrium loading through chromatographic breakthrough experiments. The chapter also explores the characterisation of a 3D-printed monolith adsorbent, highlighting their advantages in adsorption efficiency, and further reaches into adsorption equilibrium isotherm models, detailing the Langmuir model, Dual-site Langmuir (DSL) model, Sips model and Dual-site Sips (DSS) model, which are widely used to describe adsorption equilibria.

3.1 Gas Chromatography Method

Chromatography is a fundamental analytical technique extensively used in various scientific fields, including gas adsorption studies. The method allows the separation of complex mixtures into individual components, which can be further analyzed to understand their properties. In the context of gas adsorption, chromatography is crucial for identifying and quantifying gases like CH_4 and CO_2 in shale formations. This technique's ability to dissect complex gas mixtures makes it indispensable for research focused on understanding gas behaviour in different materials. The column is operated with a mixed carrier containing the adsorbable component (CH_4) and a non-adsorbable gas (Helium) in known proportions, and retention times are measured for small pulses of the adsorbable component at a series of different carrier compositions.

In gas adsorption research, particularly in the study of shale gas and CO_2 sequestration [69], chromatography plays a vital role. The method is employed to analyze the composition of gas samples after adsorption experiments, helping to determine the types and quantities of gases adsorbed onto shale. This information is critical in evaluating the efficiency and capacity of shale formations to adsorb gases. The precision offered by chromatography in measuring these quantities makes it a preferred method in many studies.

A critical aspect of chromatography in gas adsorption is the use of the Moment Method. The Moment Method is employed to analyze the data obtained from chromatographic experiments, particularly to determine the adsorption capacity, the heat of adsorption, and other thermodynamic properties. This method involves calculating the moments of the response curve obtained from the chromatograph. By integrating these moments, researchers can extract valuable information about the adsorption process, such as the amount of gas adsorbed and the rate at which equilibrium is reached. The Moment Method enhances the understanding of adsorption dynamics, making it a powerful tool alongside traditional chromatographic analysis.

Furthermore, breakthrough curves are an essential tool in gas adsorption studies, often used in conjunction with chromatographic methods. A breakthrough curve represents the concentration of a specific gas as a function of time as it exits an adsorption column. When a gas mixture is passed through an adsorption column, different gases are adsorbed at different rates, leading to a characteristic curve as the adsorbent becomes saturated. The shape and position of the breakthrough curve provide insights into the adsorbent's capacity, selectivity, and the kinetics of the adsorption process. Breakthrough curves are particularly useful for understanding how an adsorbent material performs under continuous flow conditions, which is critical for practical applications in gas separation and purification [56]. The average retention time reflects the adsorption equilibrium, which corresponds to the Henry's Law constant. In contrast, the spread of the response peak is influenced by both mass transfer resistance and axial mixing within the column. By performing measurements under various conditions, it's possible to distinguish the individual impacts of mass transfer resistance and axial mixing on the peak broadening.

The importance of the chromatographic method in adsorption processes extends beyond its technical capabilities. It is a versatile and cost-effective technique, applicable to a wide range of adsorbates and adsorbents. Whether studying simple single-component systems or more complex mixtures, chromatography provides reliable and accurate data that is essential for designing effective adsorption systems. Its adaptability makes it a valuable tool in various fields, from industrial gas separation and purification to environmental

monitoring and protection. The method's role in carbon capture and storage technologies is particularly significant, as it helps identify and optimize materials capable of selectively adsorbing carbon dioxide, a major greenhouse gas. In this context, the chromatographic method contributes to the development of more efficient processes to mitigate climate change, highlighting its critical role in both scientific research and practical applications.

3.2 Breakthrough Experimental Apparatus

The experimental apparatus and procedures employed in this study were adapted from the methods described by Zafanelli [70].

The experimental apparatus developed consists of three main sections: (a) gas preparation, (b) adsorption column, and (c) analytical gas. For the analytical section, an Agilent 6890 (G1530A) Plus Gas Chromatograph (GC) was employed to quantify the composition of the gas mixtures. This GC is equipped with advanced detection capabilities and provides precise and reliable measurements, ensuring accurate analysis of the adsorption and breakthrough experiments. In the gas preparation section, the partial pressures of CH_4, H_2, and their mixtures are established before introducing the gases into the adsorption column. Four mass flow controllers (MFC 1–4; Bronkhorst High-Tech B.V., Netherlands) regulate the flow rates of the inert gas (He), carrier gas (He or N_2), and adsorbate gases (H_2 and CH_4) to the desired levels. Additionally, the adsorption column's pressure is regulated by a back-pressure controller (BPC 1; Bronkhorst High-Tech B.V., Netherlands), while a separate BPC ensures the inlet pressure is maintained at the desired level (BPC 2; Bronkhorst High-Tech B.V., Netherlands).

As illustrated in Figure 3.1, the CH_4 and H_2 mixture enters valve V1 through line 1, where BPC 2 measures the inlet pressure of the experiment before the gas exits to the vent. Simultaneously, an inert gas flows through lines 3 and 4 to remove any residual molecules in the column, keeping it clean and ensuring a constant system flow, which is crucial for preventing fluctuations in BPC 1. Meanwhile, a carrier gas enters the system via line 5 and flows directly to BPC 1. The inert gas combines with the adsorbate species and

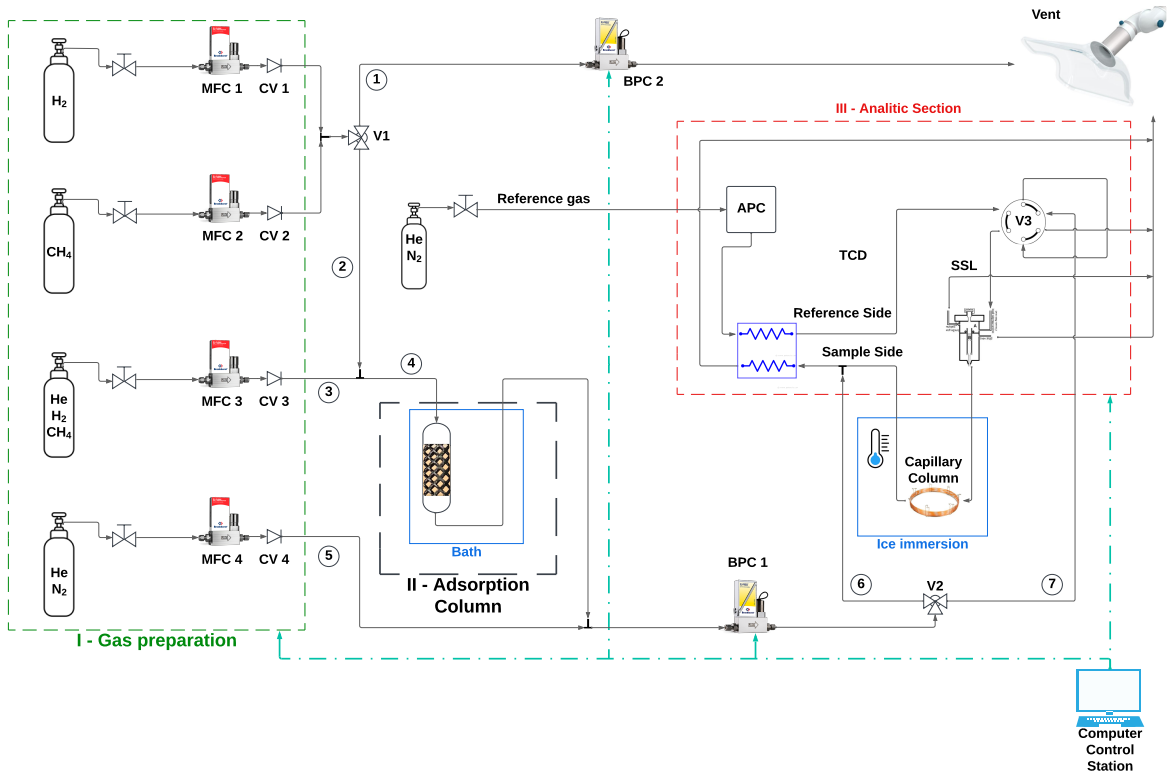

Figure 3.1: Schematic diagram of the fixed-bed apparatus used for experiments. MFC mass flow controller; BPC back pressure controller; V1, V2 and V3 valves (V1 and V2: 3-way valve, V3: 6-way valve); CV1, CV2, CV3 and CV4 check valves; Advanced Pneumatic Control; Thermal conductivity detector ; Capillary column (Molar sieve 5A-plot).

carrier gas before passing through BPC 1 and is vented through line 7. Before initiating the experiment, helium (MFC3) is shut off, and any remaining helium in the column is displaced by the adsorbate molecules.

In the adsorption section, the setup includes the same stainless-steel adsorption column with an internal diameter of 0.008 m and a length of 0.078 m, heated by a heat transfer fluid circulated through a bath equipped with a pump to maintain a constant and uniform temperature. Three standard experimental temperatures, 303 K, 313 K, and 343 K, are achieved using this heating process.

Once temperature, pressure, and flow rates are set, experiments are initiated by adjusting valve V1. Adsorbate species flow into the adsorption column through line 4,

pass through the BPC, and either proceed directly to the thermal conductivity detector (TCD) via line 6 for single-component experiments or route to sample valve V3 via line 7 for multi-component experiments. For the CH_4 and He experiments case, valve V3 switches positions every 5 seconds between "load" and "inject" and every 10 seconds between "inject" and "load". And for H_2 and N_2 experiments, valve V3 switches positions every 10 seconds between "load" and "inject" and every 10 seconds between "inject" and "load". In the "load" position, the CH_4/H_2 mixture flows into valve V4, fills the 5 μL sample loop, and vents. In the "inject" position, the carrier gas pushes the trapped sample through the split/splitless injector (operating at 423 K with a 1:100 dilution) into a capillary column (Molar Sieve 5A-Plot; 45 m length, 0.53 mm ID, 50 μm film thickness) immersed in an ice-water bath for better separation of component peaks, before analysis in the TCD at 423 K. Additionally, MFC3 can supply a pure flow of He, H_2, or CH_4, allowing experiments to begin with the column saturated with a specific gas.

3.2.1 Experimental Procedures

Before the first run, the adsorption column is activated for 12 hours at 423 K under vacuum and pure helium flows (5 mL/min). This activation step under high temperature and vacuum is critical to remove any pre-absorbed components, such as water. The weight of the column before and after the activation was noted to define the amount of dehydrated water.

To prepare the gases, the flow rates of both carrier gas (He/N_2) and adsorbate gases (CH_4/H_2) are adjusted using the Mass flow controller (MFC) so that the desired partial pressure is achieved when both gases are mixed. The total pressure is set and taken into account using the Back pressure controller (BPC).

The gas preparation section involves blending gases, for instance as helium, hydrogen, nitrogen, and methane using mass flow controllers (MFCs) for precise flow regulation. Before entering the adsorption column, the prepared gas mixture is directed through control valves to ensure proper monitoring and flow routing. Initially, it is recommended

to keep the gas mixture on the bypass side (V3) while monitoring the reference and sample gas concentrations. This ensures the stabilization of the system and allows for baseline correction in the gas chromatograph.

Once the system is stable, valve (V3) is switched to direct the gas mixture through the adsorption capillary column, which is immersed in an ice bath. The adsorption column contains the material under study, and its temperature is regulated to predetermined values using the surrounding apparatus. For the initial runs, the temperature was maintained at 313 K.

The effluent gases exiting the column are directed to the thermal conductivity detector (TCD). The TCD generates electronic signals proportional to the concentration of the effluent gases. During the experiment, the adsorbate is retained within the adsorption bed, while the carrier gas passes through. As adsorption progresses, the adsorbate eventually breaks through, leading to an S-shaped curve that represents the concentration of the adsorbate over time.

This setup allows for the collection of breakthrough curves, which are analyzed to determine adsorption capacities and other performance metrics of the adsorbent material. The experiment is repeated at different temperatures (303 K, 313 K, 343 K) and partial pressures for comprehensive analysis. Between each run, the column is reactivated by heating under helium flow for at least 30 minutes to remove residual adsorbed species and ensure reproducibility of results.

3.2.2 Adsorption Equilibrium Loading Measurement by Chromatographic Breakthrough Experiments

The dynamic equilibrium loading, q_{exp} $(mol.kg^{-1})$, in breakthrough experiments can be obtained by the following equation 3.1, which is based on the integration of the molar flow profiles of the breakthrough curves [71]:

$$q_{exp} = \frac{1}{m_{\text{ads}}} \left(F_f t_s - \int_0^{t_s} F dt - \varepsilon_b V_{ac} C_f \right) \tag{3.1}$$

where m_{ads} (kg) represents the mass of the adsorbent, F_f and F $(mol.s^{-}1)$ denotes the molar flow rate of adsorbate species in the feed inlet and outlet of the column respectively, t_s (s) is the saturation time, ε_b indicates the bed porosity, V_{ac} (m^3) is the adsorption volume of the column, and C_f $(mol.m^{-3})$ is the concentration of the feed gas-phase at the inlet of the fixed bed.

3.3 3D Printed Monolith Material and Characterization

The material was synthesized by Silva *et al.* (2024) [72] following a procedure recently developed by Steldinger *et al.* [73], which is based on stereographically (SLA) 3D printing of a porous polymer and transformed into activated carbon by thermal treatment. Accordingly, it consists of 4 main steps of resin preparation, photopolymerization, porogen extraction and thermal treatment, as shown in Figure 3.2:

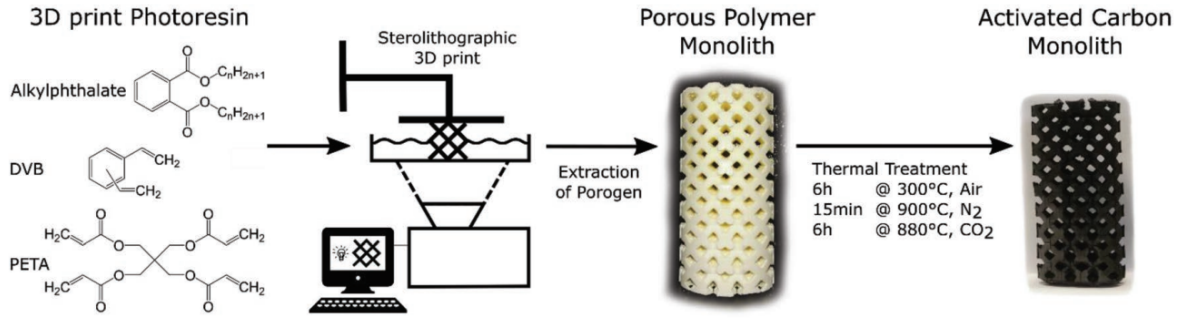

Figure 3.2: Schematic overview of the 3D printing process, starting from the liquid photoresin, then producing a porous polymer open cell structure (tetragonal unit cell) by stereolithographic 3D print and subsequent extraction of the porogen phase, finally yielding an activated carbon open cell structure upon a thermal treatment consisting of stabilization in air, pyrolysis in nitrogen and activation in CO_2.[73]

The synthesis involved 3D printing a photoresin using stereolithography technology (Kudo Titan 2HR printer) and subsequent carbonization under optimized conditions. The photoresin was composed of pentaerythritol tetraacrylate (PETA), divinylbenzene (DVB),

bis(2-ethylhexyl) phthalate (DOctP) as a porogen, Sudan-I as a dye, and phenylbis(2,4,6-trimethylbenzoyl) phosphine oxide (BAPO) as a photoinitiator. The monolith (length = 70 mm, diameter = 13.85 mm) is a reticular structure with tetragonal unit cells (5.7 × 5.7 mm) which consist of four crossed rods (r = 0.7 mm) tracing the diagonals of the cube unit cell, achieving a monolithic void fraction of 69.3 %. After printing, Soxhlet extraction with acetone for 24 hours removed porogen and dye, followed by overnight drying at 60 °C. Thermal treatments included oxidative stabilization in air at 300 °C for 6 hours (544 $mL.h^{-1}$) with a heating rate of 10 $°C.min^{-1}$, pyrolysis under nitrogen at 900 °C for 0.3 hours (10 $NL.h^{-1}$) with a heating rate of 3.3 $°C.min^{-1}$, and CO_2 activation at 860 °C for 6 hours (30 $NL.h^{-1}$) with a heating rate of 10 $°C.min^{-1}$, yielding carbon monoliths with tailored porosity and structure.

Figure 3.3: Single piece of the 3D-printed monolith

The Carbon Monolith used in this work is shown in Figure 3.3 and was namely S1. The monolith polymer was printed using W2P Solflex 350 with varied illumination time (s) and 100 μm z-axis resolution. The material had an initial mass of 3.8661 g before the thermal treatment and a final mass of 1.0806 g after the treatment, resulting in a mass loss of 72.05 %. Additionally, the monolith, with a final length of 7.8 cm, was produced using the *slow ramping program* for temperature ramping, which proved effective in producing high-quality carbon monoliths.

3.4 Modeling Adsorption Equilibrium Isotherm

3.4.1 Langmuir Isotherm

To model the adsorption equilibrium of single gases, the Langmuir equation is widely used and studied due to its simplicity, using only two parameters, and getting great accuracy for various adsorbents [56, 74, 75].

This model is based on four fundamental assumptions. The initial assumption is that the adsorbent surface is homogeneous, which implies that the energy across all adsorption sites is uniform. Secondly, it is proposed that interactions between the adsorbate particles are insignificant. Thirdly, it is assumed that each adsorption site is capable of holding only a single adsorbate molecule. In conclusion, the model considers that the equilibrium state of adsorption is in fact dynamic, with the rate of adsorption being equal to the rate of desorption from the surface [71].

The Langmuir model for a single component can be represented by the following equation 3.2 [76]:

$$q_m = q_{sat}\frac{bp}{1+bp} \tag{3.2}$$

where q_m $(mol.kg^{-1})$ represents the adsorbed concentration at equilibrium conditions, q_{sat} $(mol.kg^{-1})$ denotes the maximum saturation capacity, p (bar) is the partial pressure of adsorbate species, and b (bar^{-1}) is the adsorption affinity constant, which reflects the strength of attraction between the adsorbate molecule and the adsorbent surface.

The temperature dependence of the affinity constant follows a Van't Hoff equation 3.3:

$$b = b_\infty e^{(-\Delta H/RT)} \tag{3.3}$$

where b_∞ (bar^{-1}) represents the pre-exponential factor of the affinity constant at infinite temperature, R $(J.mol^{-1}.K^{-1})$ is the ideal gas constant, $-\Delta H$ $(J.mol^{-1})$ denotes the heat of adsorption, and T (K) is the temperature. Since adsorption is an exothermic process, the constant b decreases as the temperature increases, and so ΔH is negative.

3.4.2 DSL Isotherm

The Langmuir theory can also be applied to describe the adsorption phenomena on surfaces that offer more than one type of elementary binding sites. Considering two-types of binding sites, the contribution of each site to the total loading is simply additive, leading to the DSL isotherm [77]. All of the assumptions of the Langmuir model apply to each site. Furthermore, the sites are independents (do not interact with each other) and energetically different. The DSL model for a single component is expressed by the following equation 3.4:

$$q_m = (q_{sat1}\frac{b_1 p}{1+b_1 p})_{site1} + (q_{sat2}\frac{b_2 p}{1+b_2 p})_{site2} \tag{3.4}$$

3.4.3 Sips Model

The Sips isotherm, an empirical model that combines the characteristics of both Langmuir and Freundlich models, is particularly effective for describing Type I isotherms, which are commonly observed in commercial zeolites [63]. This flexibility makes the Sips model highly suitable for modelling gas adsorption equilibria and optimizing adsorption process designs. Its formulation provides an enhanced ability to account for heterogeneity in adsorption systems, serving as a valuable tool for more complex adsorption studies. It is defined by Equation 3.5:

$$q_m = \frac{q_{sat}\,(bp)^{1/n}}{1+(bp)^{1/n}} \tag{3.5}$$

where n is a parameter that evaluates the degree of heterogeneity of the adsorbent, typically greater than one. The larger this parameter, the more heterogeneous the system is. Based on this concept, the exponent n may take the corresponding theoretical Equation 3.6:

$$\frac{1}{n} = \frac{1}{n_0} + \alpha\left(1-\frac{T_0}{T}\right) \tag{3.6}$$

where n_0 is the parameter n at some reference temperature, α is a constant parameter and T_0 is the reference temperature.

3.4.4 Dual-site Sips Model

The Dual Site Sips model was explored in this work due to its ability to describe adsorption processes more accurately than the single-site Sips model. This approach considers adsorption on two distinct types of sites, each with its own set of parameters, providing a more flexible framework for modelling systems with heterogeneous adsorbent surfaces.

The DSS model combines the Sips isotherm with the concept of dual adsorption sites. This is expressed by Equation 3.7:

$$q_m = (q_{sat1}\frac{(b_1 p)^{1/n_1}}{1+(b_1 p)^{1/n_1}})_{site1} + (q_{sat2}\frac{(b_2 p)^{1/n_2}}{1+(b_2 p)^{1/n_2}})_{site2} \tag{3.7}$$

3.4.5 Isosteric Heat

The isosteric heat (ΔH_{st}) is defined as the ratio of the infinitesimal change in adsorbate enthalpy to the infinitesimal change in the amount adsorbed. It is described by the following thermodynamic Van't Hoff equation 3.8 [78]:

$$\frac{\Delta H_{st}}{RT^2} = \left(\frac{\partial \ln p}{\partial T}\right)_{q_{exp}} \tag{3.8}$$

Assuming that ΔH_{st} is independent of temperature, the isosteric heat can be determined directly by integrating equation 3.8 at a constant coverage. This is done using experimentally obtained adsorption isotherms, typically plotted as $\ln\ p$ versus $1/T$ as seem in Equation 3.9 [79].

$$\ln p = \text{constant} - \frac{\Delta H_{\text{st}}}{RT} \tag{3.9}$$

The variation in the heat of adsorption with regard to loading is dependent upon

the intermolecular interactions between the adsorbent and the adsorbate. Higher values of isosteric heat indicate stronger interactions and can also provide insights into the material's heterogeneous behaviour [80].

This trend can be anticipated or calculated numerically by differentiating the DSL model Equation (3.4), assuming constant loading ($dq = 0$), and substituting the result into the isosteric heat equation (3.8). This yields the following equation 3.10 [70, 71, 81]:

$$(\Delta H_{\mathrm{st}}) = \frac{q_{sat1}\frac{b_1(-\Delta H_1)}{(1+b_1p)^2} + q_{sat2}\frac{b_2(-\Delta H_2)}{(1+b_2p)^2}}{q_{sat1}\frac{b_1}{(1+b_1p)^2} + q_{sat2}\frac{b_2}{(1+b_2p)^2}} \tag{3.10}$$

For this reason, this numerical solution can be utilized to predict how the isosteric heat changes with loading, based on the heterogeneity of the adsorbent. In scenarios where the adsorption sites on the surface are identical, reflecting a homogeneous material as assumed in the Langmuir model, the isosteric heat value remains constant [81].

3.4.6 Error Estimation

The parameters for the isotherm models were determined using an optimization procedure that minimizes the mean relative deviation $\Delta\overline{q}$ between the experimental data and the model predictions, serving as the convergence criterion. The error estimation is described by the following Equation 3.11:

$$\Delta\overline{q} = \frac{1}{N}\sum\left(q_{\mathrm{exp}} - q_{\mathrm{m}}\right)^2 \tag{3.11}$$

where N is the total number of data points (experimental loadings).

Chapter 4

Results and Discussion

This chapter presents the results obtained from the experiments conducted in the studied carbon monolith. The main focus is on analysing the efficiency of the material for the separation of methane and hydrogen and their mixtures.

Single-component adsorption measurements with H_2 were performed at three temperatures (303 K, 313 K, and 343 K) and total pressures of 1 bar, 5 bar, 10 bar, 20 bar, and 30 bar for each temperature. To evaluate column behaviour under H_2 conditions, experiments with the 3D-printed monolith were conducted using N_2 as an inert carrier gas. Finally, single-component adsorption experiments with CH_4 were carried out under the same temperature conditions and at total pressures of 1 bar, 5 bar, 10 bar, 20 bar, and 30 bar, using He as an inert carrier gas.

The binary adsorption behaviour of H_2 and CH_4 in S1 3D-printed carbon monolith was investigated through breakthrough experiments measured at 303.15 K and with different molar mixtures: CH_4/H_2 ratios of 75/25, 50/50, and 25/75. The experiments were performed at a total pressure of 5 bar to ensure adsorption occurred within the nonlinear region of the isotherms, where differences in material performance are more pronounced.

To ensure consistency, measured flow rates were normalized to STP conditions (298.15 K) since the bubble flow meter temperatures varied due to ambient fluctuations and the laboratory's climatic conditions.

4.1 Single Component Adsorption of H_2 in S1 3D-Printed Carbon Monolith

The single component adsorption equilibrium of H_2 in the 3D-printed carbon monolith was evaluated to complement the data obtained for CH_4 and to provide a comprehensive understanding of the monolith performance in gas separation applications. The results obtained from the breakthrough experiments conducted under various temperature and pressure conditions up to 30 bar are presented in Figure 4.1, which displays the experimental breakthrough curves for H_2, plotted as normalized molar fraction (y/y_f) against time (min), at (a) 303 K, (b) 313 K, and (c) 343 K.

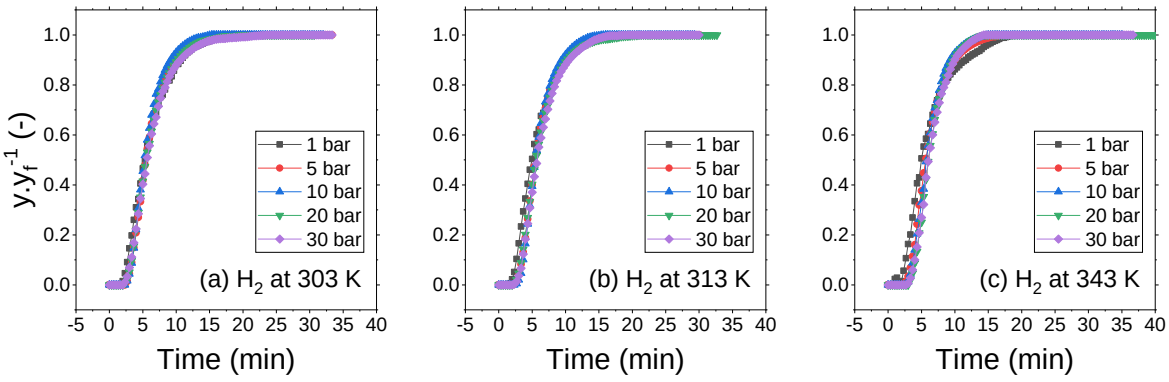

Figure 4.1: Experimental breakthrough curves of H_2 on 3D-printed monolith at (a) 303 K, (b) 313 K, (c) 343 K. The experimental conditions of each run can be found in Table 4.1.

The breakthrough curves demonstrate rapid saturation of H_2 at all tested temperatures, highlighting the lower adsorption affinity of H_2 to the monolith, as its shape remains unchanged with increasing temperature or pressure. Moreover, the experimental parameters, including flow rates, total pressures of H_2, and operating temperatures, are detailed in Table 4.1.

Additionally, the results from the H_2 adsorption runs were utilized as blank runs for the CH_4 adsorption experiments conducted on the apparatus. These blank runs enabled

the identification and subtraction of baseline effects, ensuring that the measurements for CH_4 accurately reflected its adsorption behaviour on the monolith without interference from non-adsorbing conditions.

Table 4.1: Experimental conditions of all runs at 303 K, 313 K and 343 K to study the H_2 adsorption on S1 3D-printed monolith in Agilent chromatograph.

RUNS (303.15 K)	H_2 Flow ($ml.min^{-1}$)	Total Pressure (bar)
1.1	2,35	1,00
1.2	11,4	5,00
1.3	23,1	10,0
1.4	46,2	20,0
1.5	69,4	30,0
RUNS (313.15 K)	H_2 Flow ($ml.min^{-1}$)	Total Pressure (bar)
2.1	2,23	1,00
2.2	11,3	5,00
2.3	22,5	10,0
2.4	44,8	20,0
2.5	65,7	30,0
RUNS (343.15 K)	H_2 Flow ($ml.min^{-1}$)	Total Pressure (bar)
3.1	2,24	1,00
3.2	10,3	5,00
3.3	19,9	10,0
3.4	39,8	20,0
3.5	59,8	30,0

4.2 Single Component Adsorption of CH_4 in S1 3D-Printed Carbon Monolith

The experimental parameters, including flow rates, total pressures of CH_4, system temperatures and calculated loading for the experimental runs, are provided in Table 4.2.

The results obtained from experiments conducted under varying temperature and pressure conditions are illustrated in Figure 4.2. This figure presents the experimental breakthrough curves for CH_4, plotted as the normalized molar fraction (y/y_f) versus time

Table 4.2: Experimental conditions of all runs at 303 K, 313 K and 343 K to study the CH_4 adsorption on S1 3D-printed monolith in Agilent chromatograph.

RUNS (303.15 K)	CH_4 Flow ($ml.min^{-1}$)	Total Pressure (bar)	Loading ($mol.kg^{-1}$)
1.1	2,13	1,00	1,02
1.2	11,6	5,00	2,31
1.3	23,4	10,0	2,74
1.4	45,8	20,0	3,08
1.5	66,7	30,0	3,25
RUNS (313.15 K)	CH_4 Flow ($ml.min^{-1}$)	Total Pressure (bar)	Loading ($mol.kg^{-1}$)
2.1	2,23	1,00	0,872
2.2	11,4	5,00	2,10
2.3	22,7	10,0	2,61
2.4	45,3	20,0	2,99
2.5	66,4	30,0	3,17
RUNS (343.15 K)	CH_4 Flow ($ml.min^{-1}$)	Total Pressure (bar)	Loading ($mol.kg^{-1}$)
3.1	2,03	1,00	0,496
3.2	10,4	5,00	1,62
3.3	20,4	10,0	2,22
3.4	40,1	20,0	2,71
3.5	57,0	30,0	2,93

*Utilizing the H_2 experiments as baseline for Loading

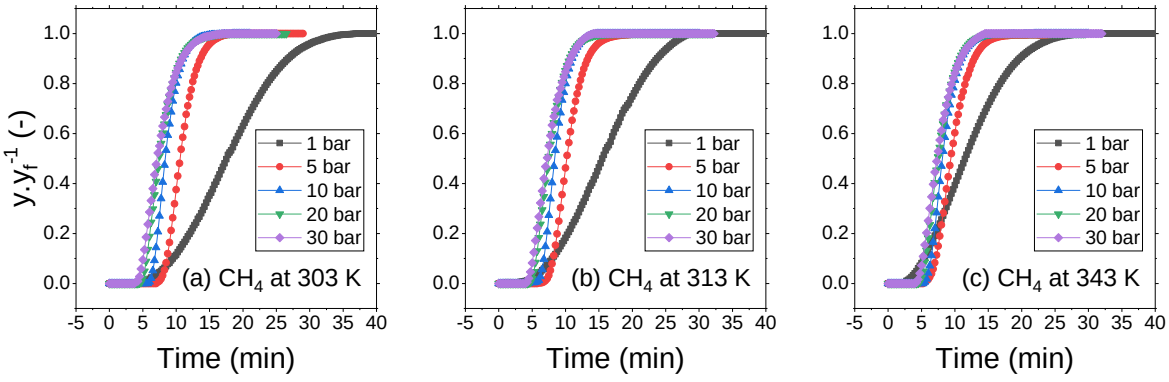

Figure 4.2: Experimental breakthrough curves of CH_4 on 3D-printed monolith at (a) 303 K, (b) 313 K, (c) 343 K and different pressures performed on Agilent 6890 GC. The experimental conditions of each run can be found in Table 4.2.

(min) at (a) 303 K, (b) 313 K, and (c) 343 K.

For CH_4, the breakthrough curves indicate delayed saturation, with the shape changing as temperature or pressure increases, thereby confirming its stronger affinity to the adsorbent and the monolith's efficiency in adsorbing CH_4. Furthermore, higher temperatures led to faster breakthrough curves, as expected, since adsorption is an exothermic phenomenon, which decreases the amount adsorbed as temperature rises. In addition, increased pressure at the feed also sharpened the breakthrough curves.

4.3 Modelling Adsorption Equilibrium Isotherms

Table 4.3 presents the parameters of different isotherm models obtained from the fitting of adsorption equilibrium data for CH_4. The results highlight the suitability of the DSL model in describing the adsorption behaviour of CH_4, particularly at higher pressures, as it provides the lowest error. The fitted parameters emphasize the potential of the studied material for CH_4 adsorption and its separation from H_2.

Table 4.3: Isotherm models parameters for sorption of CH_4 on S1 3D-printed carbon monolith.

Model	q_{sat} $(mol.kg^{-1})$		b_∞ (bar^{-1})		-ΔH (kJ mol^{-1})		n (-)		$\Delta\overline{q}$
	q_{sat1}	q_{sat2}	$b_{\infty 1}$	$b_{\infty 2}$	-ΔH_1	-ΔH_2	n_1	n_2	
Langmuir	3.44		$2.74 \cdot 10^{-4}$		18.5		1		$1.06 \cdot 10^{-3}$
DSL	3.33	1.06	$4.19 \cdot 10^{-4}$	$1.09 \cdot 10^{-5}$	17.4	15.9	1	1	$3.86 \cdot 10^{-4}$
Sips	3.49		$2.97 \cdot 10^{-4}$		18.2		1.02		$6.65 \cdot 10^{-4}$
DSS	3.38	1.51	$3.86 \cdot 10^{-4}$	$5.79 \cdot 10^{-6}$	17.6	15.9	1.02	1.02	$3.87 \cdot 10^{-4}$

As demonstrated in Figure 4.3, the experimental results for CH_4 adsorption demonstrated a consistent and accurate fit to the DSL model, indicating heterogeneous adsorption behaviour within the 3D-printed carbon monolith. The model revealed two distinct adsorption sites. Site 1 exhibited q_{sat1} of 3.33 $mol.kg^{-1}$ with $b_{\infty 1}$ of $4.19 \cdot 10^{-4}$ bar^{-1}, suggesting a site with higher affinity for CH_4. Conversely, site 2 showed q_{sat2} of 1.06 $mol.kg^{-1}$ and a significantly lower $b_{\infty 2}$ of $1.09 \cdot 10^{-5}$ bar^{-1}, indicative of a site with lower energy interactions and relevance at higher pressures.

The model also provided insight into the heterogeneity of the adsorption sites, reflected in the distinct affinity constants. These parameters are crucial for understanding the adsorption performance and highlight the potential of the carbon monolith for applications in the gas separation CH_4/H_2.

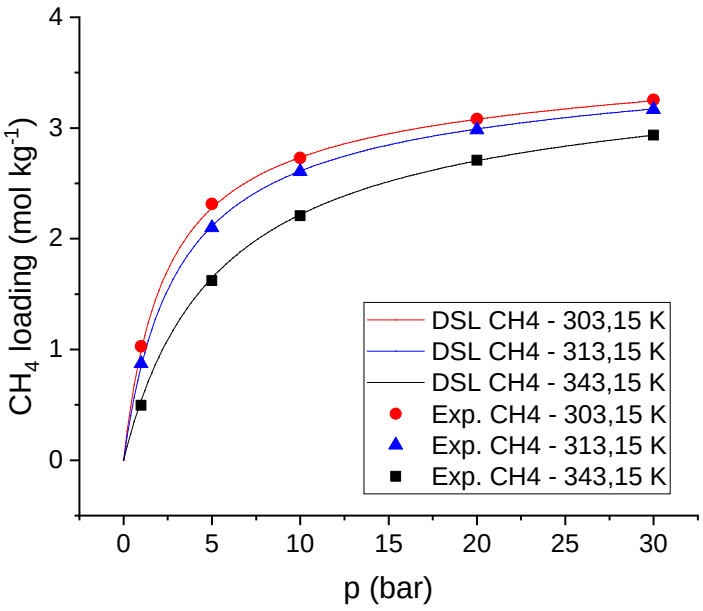

Figure 4.3: Adsorption equilibrium isotherms of CH_4 on 3D-printed carbon monolith. Symbols = experimental; Solid lines = model.

As illustrated in Figure 4.4, the adsorption results obtained in this work are compared with various studies from the literature [63, 70, 82–84], at low pressures (up to 4 bar), the 3D-printed carbon monolith exhibits a higher CH_4 adsorption capacity than Zeolite 13X and other analyzed materials. However, as the pressure increases, its performance stabilizes and approaches that of MOF MIL-160, positioning it within the range of materials commonly used for methane adsorption. At higher pressures, a direct comparison with Zeolite 13X reveals that the carbon monolith exhibits a lower adsorption capacity, as Zeolite 13X maintains a more pronounced growth trend. These results indicate that the developed material offers a promising alternative for methane adsorption, balancing adsorption performance with the benefits of 3D printing.

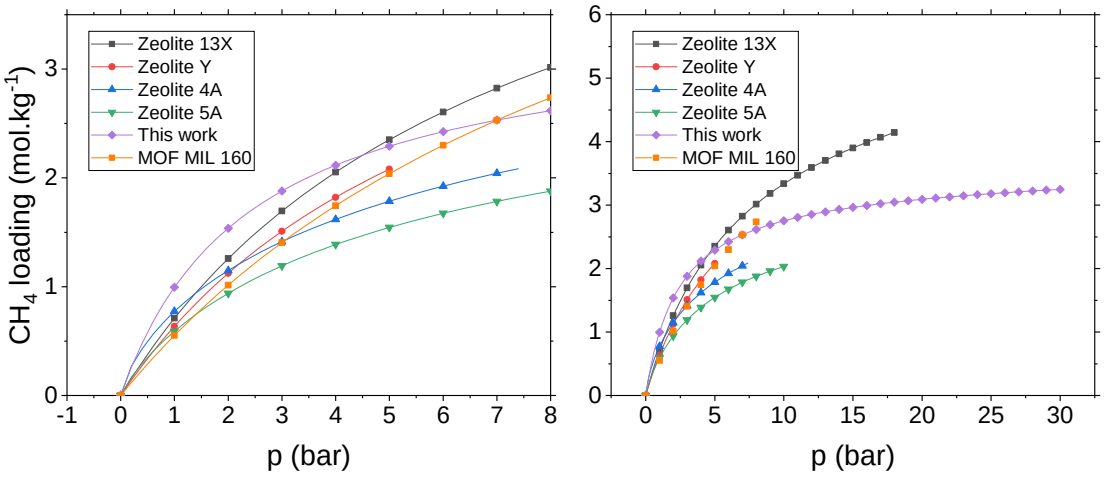

Figure 4.4: Comparison of CH_4 Adsorption Capacities for Different Adsorbents at 303 K.

This difference is supported by the parameters summarized in Table 4.4, obtained using the Langmuir, DSL, and Sips models. The monolith exhibits a q_{sat} value of 3.33 $mol.kg^{-1}$, which is lower than that of Zeolite 13X (5.12 $mol.kg^{-1}$), indicating a reduced saturation capacity at the main adsorption sites. Additionally, the affinity coefficients (b) are higher, while the adsorption enthalpy values (ΔH) remain similar. This suggest that methane interacts rapidly with the porous carbon monolith compared to Zeolite 13X but with similar energy, potentially leading to comparable efficiency under specific operational conditions.

Table 4.4: Comparison of isotherm model parameters for different materials at 303 K

Reference	Material	q_{sat} $(mol.kg^{-1})$		b (bar^{-1})		-ΔH (kJ mol^{-1})		n (-)
		q_{sat1}	q_{sat2}	b_1	b_2	-ΔH_1	-ΔH_2	
[63]	Zeolite 4A	4.16		$1.36 \cdot 10^{-1}$		19.5		
[70]	Zeolite 13X	2.13	5.12	$1.20 \cdot 10^{-2}$	$1.54 \cdot 10^{-1}$	16.1	18.0	
[82]	Zeolite Y	4.18		$1.52 \cdot 10^{-1}$		16.9		
[83]	MOF MIL-160	5.25	1.29	$7.90 \cdot 10^{-2}$	$1.50 \cdot 10^{-1}$	12.1	5.20	
[84]	Zeolite 5A	3.28		$1.75 \cdot 10^{-1}$		16.1		0.87
This work	3D Carbon Monolith	3.33	1.06	$4.22 \cdot 10^{-1}$	$5.99 \cdot 10^{-3}$	17.4	15.9	

Despite these differences, the results indicate that the 3D-printed carbon monolith offers competitive and well-balanced performance, establishing itself as a viable alternative

for methane adsorption, combining good adsorption properties with the advantages of additive manufacturing.

It is important to note that the literature data were obtained from adsorption curves calculated using the respective models employed in those studies and extrapolated to 303 K for comparison. This adjustment provides a consistent basis for evaluating material performance under equivalent conditions. The extrapolations were carried out up to the highest pressures used in these studies to avoid any inaccurate information.

This comparison reinforces the efficiency and applicability of the monolith, validating its adsorption performance regardless of the differences in experimental setup.

4.4 Isosteric Heat of Adsorption in a 3D-Printed Carbon Monolith

The behaviour of isosteric heat of adsorption as a function of loading was predicted by applying Equation 3.4 (from the DSL isotherm) and showed in Figure 4.5. Since the model assumes that all active sites are energetically equal, resulting in a constant isosteric heat regardless of loading. However, when considering the overall adsorption process across both site types, the total isosteric heat can vary with loading due to the differing energies of the two sites.

This demonstrates consistent performance across a range of loadings and temperatures. In the left graph, the values around 17.5 $kJ.mol^{-1}$ and 17.1 $kJ.mol^{-1}$ up to a loading of 2.93 $mol.kg^{-1}$ suggest a moderate physisorption mechanism. This indicates a balance between efficient adsorption for effective gas capture and facile desorption, facilitating material regeneration. In the right graph, the slope remains nearly constant, with isosteric heat values of 17.2 $kJ.mol^{-1}$ at a loading of 2.93 $mol.kg^{-1}$, 17.3 $kJ.mol^{-1}$ at 2.50 $mol.kg^{-1}$, and 17.4 $kJ.mol^{-1}$ at both 2.00 $mol.kg^{-1}$ and 1.50 $mol.kg^{-1}$. This stability across different temperatures highlights the material's thermal robustness, making it a promising candidate for gas separation applications under dynamic operational

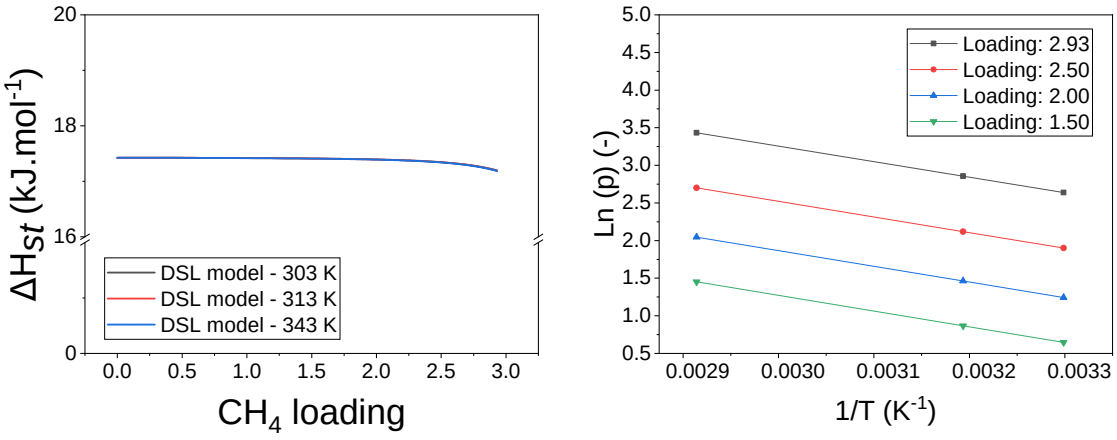

Figure 4.5: Isosteric heat of adsorption as a function of coverage for CH_4 on 3D printed monolith.

conditions.

The slight decrease in the isosteric heat with increasing loading suggests minor heterogeneity in the adsorption sites, where higher-energy sites are occupied first, followed by lower-energy sites. As noted by Do [85], this decrease in heat of adsorption with loading indicates the presence of adsorption sites with varying energy levels.

The isosteric heat of adsorption (ΔH_{st}) is a key thermodynamic parameter that offers insights into the strength of interaction between the adsorbate and the adsorbent surface. High values of ΔH_{st} indicate strong interactions, which are desirable for applications requiring selective adsorption, such as gas separation or purification. In contrast, moderate values ensure easier desorption, which is beneficial for cyclic processes like Pressure Swing Adsorption (PSA) and Temperature Swing Adsorption (TSA).

4.5 Binary Adsorption of H_2 and CH_4 in S1 3D-Printed Carbon Monolith

The adsorption of H_2 and CH_4 on the S1 3D-printed carbon monolith was investigated through binary breakthrough experiments at 303.15 K and a total pressure of 5 bar, using

CH_4/H_2 molar ratios of 75/25, 50/50, and 25/75 to simulate hydrogen blending scenarios in natural gas pipelines. Prior to the gas mixture introduction, the adsorption column was saturated with pure H_2 to ensure the experiments were conducted under conditions that allowed adsorption to occur within the nonlinear region of the isotherms, where material performance differences are more pronounced, as detailed in Table 4.5.

Table 4.5: Experimental conditions of all runs at 303 K to study the binary adsorption of CH_4 and H_2 on S1 3D-printed monolith in Agilent chromatograph.

RUNS	CH_4 Flow ($ml.min^{-1}$)	H_2 Flow ($ml.min^{-1}$)	% CH_4	% H_2	Total Pressure (bar)	Partial Pressure of CH_4 (bar)	Loading of CH_4 ($mol.kg^{-1}$)
B1	9,17	2,82	76%	24%	5,00	3,83	2,10
B2	6,13	6,12	50%	50%	5,00	2,50	1,71
B3	3,05	2,82	26%	74%	5,00	1,30	1,20

As shown in Figure 4.6, the binary breakthrough curves for CH_4/H_2 on the S1 3D-Printed Carbon Monolith showed a clear dependence on partial pressure. As the pressure increased, the breakthrough time consistently decreased across all CH_4/H_2 ratios, which reflects the adsorption behaviour of CH_4 on the S1 monolith. Consequently, the breakthrough time and experimental mixture ratios were observed to be 1.75 minutes in the 76/24 mixture, 2.00 minutes in the 50/50 mixture, and 2.50 minutes in the 26/74 mixture.

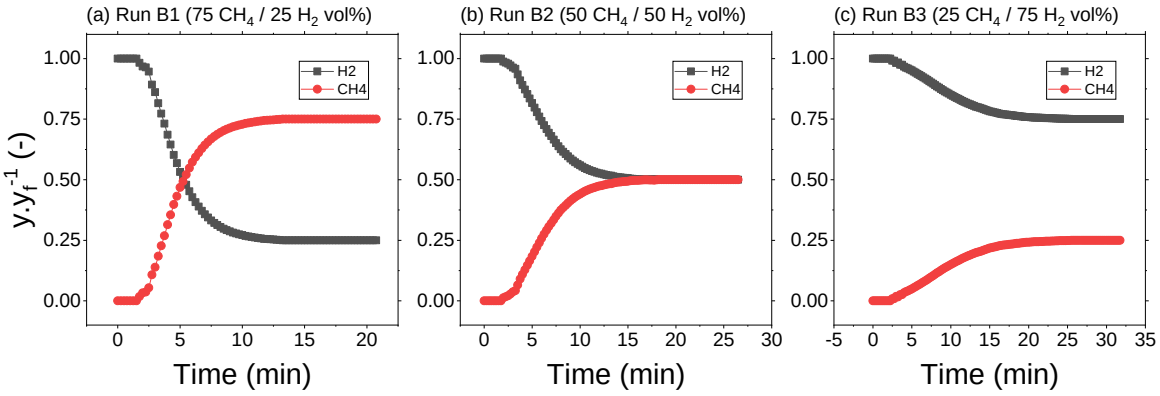

Figure 4.6: Adsorption breakthrough curves for calculated mixture ratios CH_4/H_2 of (a) (75/25 vol%), (b) (50/50 vol%) and (c) (25/75 vol%) on S1 3D-Printed Carbon Monolith at 303.15 K and 05 bar.

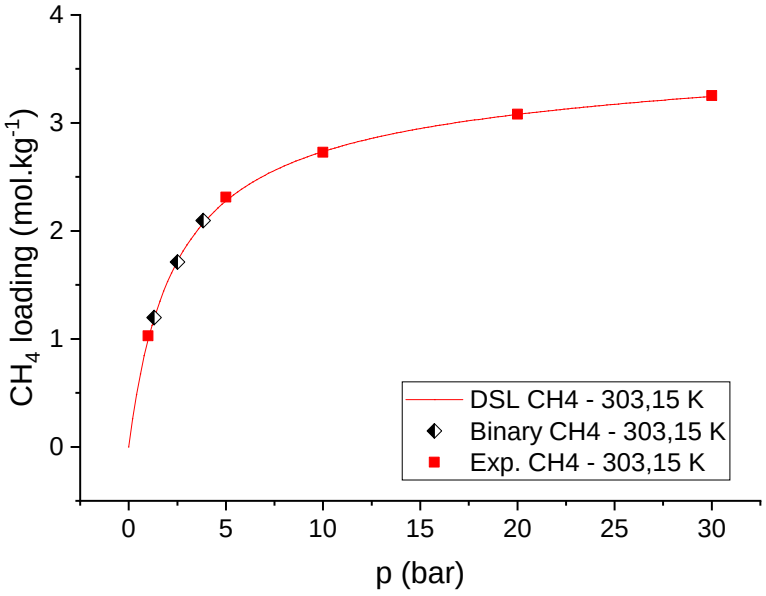

Figure 4.7: Adsorption equilibrium of binary experiments of CH_4 on 3D-printed carbon monolith. Symbols = experimental; Solid lines = model.

As evidenced in figure 4.7, this behaviour reinforces the material's potential for selective CH_4 separation. The adsorbed amounts were 2.10, 1.71, and 1.20 $mol.kg^{-1}$ for the 76/24, 50/50, and 26/74 mixtures, respectively, closely matching the values predicted by the DSL model from the single component experiments, further validating its applicability. These results highlight the higher adsorption affinity of the S1 monolith for CH_4 and its negligible adsorption of H_2, making it a promising candidate for natural gas purification and hydrogen separation.

Chapter 5

Conclusion and Future Work

This study presents an experimental investigation of CH_4 and H_2 adsorption on a 3D-printed porous carbon monolith, designed to enhance the selective separation of these gases. Single-component and binary adsorption experiments, conducted in a fixed-bed system with flow gas chromatography, demonstrated that the evaluated monolith exhibits high selectivity for CH_4, while H_2 adsorption was negligible under all tested conditions.

The experimental data were correlated with the DSL isotherm model, with the fitted parameters determined as 3.33 $mol.kg^{-1}$ at site 1 and 1.06 $mol.kg^{-1}$ at site 2. The equilibrium isotherms confirmed the presence of heterogeneous adsorption sites, while the isosteric heat of adsorption ranged from 17.5 to 17.1 $kJ.mol^{-1}$, indicating a moderate physisorption mechanism.

Binary CH_4/H_2 experiments conducted at 303 K and 5 bar further reinforced the material's selectivity, with CH_4 adsorption reaching 2.10 $mol.kg^{-1}$ for a 76/24 (% vol.) gas mixture. This result aligns with the single-component adsorption data, demonstrating that the presence of H_2 in the system does not alter the amount of CH_4 adsorbed, confirming its negligible effect. These observations validate the applicability of the monolith for H_2 purification processes in methane reforming, highlighting its robustness as a selective adsorbent in gas separation.

Based on the outcomes of this work, future investigations could explore binary adsorption experiments at higher pressures, such as 30 bar, to evaluate the monolith's performance under more industrially relevant conditions. Additionally, this material shows potential for CO_2 capture from post-combustion streams, as CO_2 molecules are larger than CH_4 and tend to exhibit stronger interactions with adsorbents. Therefore, evaluating its ability to selectively capture CO_2 in CH_4/N_2 mixtures could provide valuable insights into its feasibility for greenhouse gas mitigation and its potential contribution to advancing sustainable carbon capture technologies.

Bibliography

[1] GlobeNewswire, "Gas separation membrane market poised for continued growth," *GlobeNewswire*, 2025, Accessed: January 26, 2025. [Online]. Available: https://www.globenewswire.com/news-release/2025/01/03/3003908/28124/en/Gas-Separation-Membrane-Market-Poised-for-Continued-Growth-Expected-to-Surpass-3-Billion-by-2028-Global-Forecast-to-2033.html.

[2] T. M. Research, "Global zeolite membrane market poised for expansion," *GlobeNewswire*, 2025, Accessed: January 26, 2025. [Online]. Available: https://www.globenewswire.com/news-release/2025/01/16/3010906/32656/en/Global-Zeolite-Membrane-Market-Poised-for-Expansion-Reaching-743-6-Million-by-2034-Transparency-Market-Research.html.

[3] C. Song, Q. Liu, N. Ji, Y. Kansha, and A. Tsutsumi, "Optimization of steam methane reforming coupled with pressure swing adsorption hydrogen production process by heat integration," *Applied energy*, vol. 154, pp. 392–401, 2015.

[4] M. Amin *et al.*, "Issues and challenges in hydrogen separation technologies," *Energy Reports*, vol. 9, pp. 894–911, 2023.

[5] P. Holzmann, R. J. Breitenecker, A. A. Soomro, and E. J. Schwarz, "User entrepreneur business models in 3d printing," *Journal of Manufacturing Technology Management*, vol. 28, no. 1, pp. 75–94, 2017.

[6] S. A. Tofail, E. P. Koumoulos, A. Bandyopadhyay, S. Bose, L. O'Donoghue, and C. Charitidis, "Additive manufacturing: Scientific and technological challenges, market uptake and opportunities," *Materials today*, vol. 21, no. 1, pp. 22–37, 2018.

[7] Ö. Keleş, C. W. Blevins, and K. J. Bowman, "Effect of build orientation on the mechanical reliability of 3d printed abs," *Rapid Prototyping Journal*, vol. 23, no. 2, pp. 320–328, 2017.

[8] C. Murray, "Common applications of 3d printing: From aerospace to fashion," *Forbes*, 2023, Accessed: January 26, 2025. [Online]. Available: `https://www.forbes.com/sites/conormurray/2023/04/21/common-applications-of-3d-printing-from-aerospace-to-fashion/`.

[9] N. Shahrubudin, T. C. Lee, and R. Ramlan, "An overview on 3d printing technology: Technological, materials, and applications," *Procedia manufacturing*, vol. 35, pp. 1286–1296, 2019.

[10] A. Standard *et al.*, "Standard terminology for additive manufacturing technologies," *ASTM International F2792-12a*, vol. 46, pp. 10 918–10 928, 2012.

[11] S. Vijayavenkataraman, J. Y. Fuh, and W. F. Lu, "3d printing and 3d bioprinting in pediatrics," *Bioengineering*, vol. 4, no. 3, p. 63, 2017.

[12] A. Müller and S. Karevska, "How will 3d printing make your company the strongest link in the value chain," *EY's Global 3D printing Report*, vol. 2016, 2016.

[13] U. M. Dilberoglu, B. Gharehpapagh, U. Yaman, and M. Dolen, "The role of additive manufacturing in the era of industry 4.0," *Procedia manufacturing*, vol. 11, pp. 545–554, 2017.

[14] J. W. Stansbury and M. J. Idacavage, "3d printing with polymers: Challenges among expanding options and opportunities," *Dental materials*, vol. 32, no. 1, pp. 54–64, 2016.

[15] C. L. Ventola, "Medical applications for 3d printing: Current and projected uses," *Pharmacy and Therapeutics*, vol. 39, no. 10, p. 704, 2014.

[16] Z.-X. Low, Y. T. Chua, B. M. Ray, D. Mattia, I. S. Metcalfe, and D. A. Patterson, "Perspective on 3d printing of separation membranes and comparison to related unconventional fabrication techniques," *Journal of membrane science*, vol. 523, pp. 596–613, 2017.

[17] J. E. Bara, C. I. Hawkins, D. T. Neuberger, and S. W. Poppell, "3d printing for co 2 capture and chemical engineering design," *Nanomaterials and Energy*, 2015.

[18] T. Van Gerven and A. Stankiewicz, "Structure, energy, synergy, time the fundamentals of process intensification," *Industrial & engineering chemistry research*, vol. 48, no. 5, pp. 2465–2474, 2009.

[19] C. Parra-Cabrera, C. Achille, S. Kuhn, and R. Ameloot, "3d printing in chemical engineering and catalytic technology: Structured catalysts, mixers and reactors," *Chemical Society Reviews*, vol. 47, no. 1, pp. 209–230, 2018.

[20] I. D. Amores, J. González-Gutiérrez, I. M. García, J. M. Franco, and C. Gallegos, "3d printing–present and future–a chemical engineering perspective," *Chemical Engineering Research and Design*, vol. 187, pp. 598–610, 2022.

[21] S. Bettermann, F. Kandelhard, H.-U. Moritz, and W. Pauer, "Digital and lean development method for 3d-printed reactors based on cad modeling and cfd simulation," *Chemical Engineering Research and Design*, vol. 152, pp. 71–84, 2019.

[22] K.-W. Gyak, N. K. Vishwakarma, Y.-H. Hwang, J. Kim, H.-s. Yun, and D.-P. Kim, "3d-printed monolithic sicn ceramic microreactors from a photocurable preceramic resin for the high temperature ammonia cracking process," *Reaction Chemistry & Engineering*, vol. 4, no. 8, pp. 1393–1399, 2019.

[23] M. J. Harding *et al.*, "3d printing of peek reactors for flow chemistry and continuous chemical processing," *Reaction Chemistry & Engineering*, vol. 5, no. 4, pp. 728–735, 2020.

[24] C.-G. Lin *et al.*, "Digital control of multistep hydrothermal synthesis by using 3d printed reactionware for the synthesis of metal–organic frameworks," *Angewandte Chemie*, vol. 130, no. 51, pp. 16 958–16 962, 2018.

[25] D. Zhang, J. Xiao, Q. Guo, and J. Yang, "3d-printed highly porous and reusable chitosan monoliths for cu (ii) removal," *Journal of Materials Science*, vol. 54, no. 8, pp. 6728–6741, 2019.

[26] X. Xu *et al.*, "3d-printed grids with polymeric photocatalytic system as flexible air filter," *Applied Catalysis B: Environmental*, vol. 262, p. 118 307, 2020.

[27] D. N. Mendes, A. Gaspar, I. Ferreira, J. P. Mota, and R. P. Ribeiro, "3d-printed hybrid zeolitic/carbonaceous electrically conductive adsorbent structures," *Chemical Engineering Research and Design*, vol. 174, pp. 442–453, 2021.

[28] M. N. Issac and B. Kandasubramanian, "Review of manufacturing three-dimensional-printed membranes for water treatment," *Environmental Science and Pollution Research*, vol. 27, no. 29, pp. 36 091–36 108, 2020.

[29] L. D. Tijing, J. R. C. Dizon, I. Ibrahim, A. R. N. Nisay, H. K. Shon, and R. C. Advincula, "3d printing for membrane separation, desalination and water treatment," *Applied Materials Today*, vol. 18, p. 100 486, 2020.

[30] M. N. Nadagouda, M. Ginn, and V. Rastogi, "A review of 3d printing techniques for environmental applications," *Current opinion in chemical engineering*, vol. 28, pp. 173–178, 2020.

[31] M. E. Boot-Handford *et al.*, "Carbon capture and storage update," *Energy & Environmental Science*, vol. 7, no. 1, pp. 130–189, 2014.

[32] M. Bui *et al.*, "Carbon capture and storage (ccs): The way forward," *Energy & Environmental Science*, vol. 11, no. 5, pp. 1062–1176, 2018.

[33] J. C. Pires, F. G. Martins, M. C. Alvim-Ferraz, and M. Simões, "Recent developments on carbon capture and storage: An overview," *Chemical engineering research and design*, vol. 89, no. 9, pp. 1446–1460, 2011.

[34] A. Al-Mamoori, A. Krishnamurthy, A. A. Rownaghi, and F. Rezaei, "Carbon capture and utilization update," *Energy Technology*, vol. 5, no. 6, pp. 834–849, 2017.

[35] A. Kätelhön, R. Meys, S. Deutz, S. Suh, and A. Bardow, "Climate change mitigation potential of carbon capture and utilization in the chemical industry," *Proceedings of the National Academy of Sciences*, vol. 116, no. 23, pp. 11 187–11 194, 2019.

[36] S. Shah, M. Shah, A. Shah, and M. Shah, "Evolution in the membrane-based materials and comprehensive review on carbon capture and storage in industries," *Emergent Materials*, vol. 3, no. 1, pp. 33–44, 2020.

[37] M. Houkan, O. Shehata, K. Kannan, J.-J. Cabibihan, A. M Abdullah, and K. K. Sadasivuni, "Development of in-situ sensors for co2 to fuel process," *QSpace Institutional Respository*, 2020.

[38] M. B. Haider, Z. Hussain, and R. Kumar, "Co2 absorption and kinetic study in ionic liquid amine blends," *Journal of Molecular Liquids*, vol. 224, pp. 1025–1031, 2016.

[39] A. Veawab, P. Tontiwachwuthikul, and A. Chakma, "Corrosion behavior of carbon steel in the co2 absorption process using aqueous amine solutions," *Industrial & engineering chemistry research*, vol. 38, no. 10, pp. 3917–3924, 1999.

[40] M. S. B. Reddy, D. Ponnamma, K. K. Sadasivuni, B. Kumar, and A. M. Abdullah, "Carbon dioxide adsorption based on porous materials," *RSC advances*, vol. 11, no. 21, pp. 12 658–12 681, 2021.

[41] J.-R. Li, R. J. Kuppler, and H.-C. Zhou, "Selective gas adsorption and separation in metal–organic frameworks," *Chemical Society Reviews*, vol. 38, no. 5, pp. 1477–1504, 2009.

[42] H. Furukawa, K. E. Cordova, M. O'Keeffe, and O. M. Yaghi, "The chemistry and applications of metal-organic frameworks," *Science*, vol. 341, no. 6149, p. 1 230 444, 2013.

[43] C. Y. Chaparro-Garnica, E. Bailón-García, A. Davó-Quiñonero, D. Lozano-Castello, and A. Bueno-López, "Sponge-like carbon monoliths: Porosity control of 3d-printed carbon supports and its influence on the catalytic performance," *Chemical Engineering Journal*, vol. 432, p. 134 218, 2022.

[44] J. Liu, Y. Wang, A. I. Benin, P. Jakubczak, R. R. Willis, and M. D. LeVan, "Co2/h2o adsorption equilibrium and rates on metal- organic frameworks: Hkust-1 and ni/dobdc," *Langmuir*, vol. 26, no. 17, pp. 14 301–14 307, 2010.

[45] J. G. Nguyen and S. M. Cohen, "Moisture-resistant and superhydrophobic metal-organic frameworks obtained via postsynthetic modification," *Journal of the American Chemical Society*, vol. 132, no. 13, pp. 4560–4561, 2010.

[46] R. L. Siegelman, E. J. Kim, and J. R. Long, "Porous materials for carbon dioxide separations," *Nature materials*, vol. 20, no. 8, pp. 1060–1072, 2021.

[47] A. Henrique *et al.*, "Separation of alkane isomers in a hierarchically structured 3d-printed porous carbon monolith," *Chemical Engineering Journal*, vol. 472, p. 145 138, 2023.

[48] H. Thakkar, S. Eastman, A. Hajari, A. A. Rownaghi, J. C. Knox, and F. Rezaei, "3d-printed zeolite monoliths for co2 removal from enclosed environments," *ACS applied materials & interfaces*, vol. 8, no. 41, pp. 27 753–27 761, 2016.

[49] D. Lozano-Castelló, D. Cazorla-Amorós, A. Linares-Solano, and D. Quinn, "Activated carbon monoliths for methane storage: Influence of binder," *Carbon*, vol. 40, no. 15, pp. 2817–2825, 2002.

[50] D. P. Vargas, L. Giraldo, J. Silvestre-Albero, and J. C. Moreno-Piraján, "Co 2 adsorption on binderless activated carbon monoliths," *Adsorption*, vol. 17, pp. 497–504, 2011.

[51] A. M. Najafi, S. Soltanali, F. Khorashe, and H. Ghassabzadeh, "Effect of binder on co2, ch4, and n2 adsorption behavior, structural properties, and diffusion coefficients on extruded zeolite 13x," *Chemosphere*, vol. 324, p. 138 275, 2023.

[52] X. Lu *et al.*, "Competitive adsorption of a binary co 2–ch 4 mixture in nanoporous carbons: Effects of edge-functionalization," *Nanoscale*, vol. 7, no. 3, pp. 1002–1012, 2015.

[53] J. Liu, H. Shang, J. Yang, J. Wang, J. Li, and S. Deng, "Novel zeolite/carbon monolith adsorbents for efficient ch4/n2 separation," *Chemical Engineering Journal*, vol. 426, p. 130 163, 2021.

[54] A. J. Abubakar, R. L. Canevesi, D. A. Sanchez, and C. A. Grande, "Monoliths for gas storage manufactured with precision pore engineering using 3d-printed templates," *Chemical Engineering Journal*, vol. 489, p. 151 450, 2024.

[55] K. S. W. Sing *et al.*, "Reporting physisorption data for gas/solid systems with special reference to the determination of surface area and porosity," *Pure and Applied Chemistry*, vol. 66, no. 8, pp. 1739–1758, 1994. DOI: 10.1351/pac199466081739.

[56] E. Aly, "Sorption of co2 and n2 in binder-free zeolite ky studied by a chromatographic method," Ph.D. dissertation, Escola Superior de Tecnologia de Gestão Instituto Politécnico de Bragança, 2020.

[57] Y.-J. Kang *et al.*, "A brief review of formaldehyde removal through activated carbon adsorption," *Applied Sciences*, vol. 12, no. 10, p. 5025, 2022.

[58] Y. Park, J.-H. Kang, D.-K. Moon, Y. S. Jo, and C.-H. Lee, "Parallel and series multi-bed pressure swing adsorption processes for h2 recovery from a lean hydrogen mixture," *Chemical Engineering Journal*, vol. 408, p. 127 299, 2021.

[59] J. He *et al.*, "Improving the carbon resistance of iron-based oxygen carrier for hydrogen production via chemical looping steam methane reforming: A review," *Fuel*, vol. 351, p. 128 864, 2023.

[60] S. J. Edens *et al.*, "An upper bound visualization of design trade-offs in adsorbent materials for gas separations: Co2, n2, ch4, h2, o2, xe, kr, and ar adsorbents," *Advanced Science*, vol. 10, no. 8, p. 2 206 437, 2023.

[61] M. L. Comroe, K. W. Kolasinski, and D. Saha, "Direct ink 3d printing of porous carbon monoliths for gas separations," *Molecules*, vol. 27, no. 17, p. 5653, 2022.

[62] Y.-J. Park, H. L. Choi, and T.-H. Bae, "Highly microporous activated carbons synthesized from sacrificial templating of melamine for ch4 and h2 storages and ch4/h2 adsorptive separation," *Fuel*, vol. 377, p. 132 765, 2024.

[63] M. Karimi, A. E. Rodrigues, and J. A. Silva, "Designing a simple volumetric apparatus for measuring gas adsorption equilibria and kinetics of sorption. application and validation for co2, ch4 and n2 adsorption in binder-free beads of 4a zeolite," *Chemical Engineering Journal*, vol. 425, p. 130 538, 2021.

[64] A. Streb and M. Mazzotti, "Adsorption for efficient low carbon hydrogen production: Part 1—adsorption equilibrium and breakthrough studies for h 2/co 2/ch 4 on zeolite 13x," *Adsorption*, vol. 27, pp. 541–558, 2021.

[65] T. Li *et al.*, "Tuning the pore environment of mofs toward efficient ch4/n2 separation under humid conditions," *ACS Applied Materials & Interfaces*, vol. 14, no. 13, pp. 15 830–15 839, 2022.

[66] S. Ullah *et al.*, "Synthesis and characterization of mesoporous mof umcm-1 for co2/ch4 adsorption; an experimental, isotherm modeling and thermodynamic study," *Microporous and Mesoporous Materials*, vol. 294, p. 109 844, 2020.

[67] D. M. Ruthven, *Principles of Adsorption and Adsorption Processes*. Wiley, 1984.

[68] R. T. Yang, *Adsorbents: Fundamentals and Applications*. Wiley-Interscience, 2003.

[69] M. P. Mudoi, P. Sharma, and A. S. Khichi, "A review of gas adsorption on shale and the influencing factors of ch4 and co2 adsorption," *Journal of Petroleum Science and Engineering*, vol. 217, p. 110 897, 2022.

[70] L. F. Zafanelli, E. Aly, A. E. Rodrigues, and J. A. Silva, "A novel cryogenic fixed-bed adsorption apparatus for studying green hydrogen recovery from natural gas grids," *Separation and Purification Technology*, vol. 307, p. 122 824, 2023.

[71] D. D. Do, *Adsorption analysis: Equilibria and kinetics*. World Scientific, 1998, vol. 2.

[72] A. S. Silva *et al.*, "3d printed photopolymer derived carbon catalysts for enhanced wet peroxide oxidation," *Chemical Engineering Journal*, vol. 499, p. 156 574, 2024.

[73] H. Steldinger, A. Esposito, K. Brunnengräber, J. Gläsel, and B. J. Etzold, "Activated carbon in the third dimension—3d printing of a tuned porous carbon," *Advanced Science*, vol. 6, no. 19, p. 1 901 340, 2019.

[74] J.-Y. Wang, E. Mangano, S. Brandani, and D. M. Ruthven, "A review of common practices in gravimetric and volumetric adsorption kinetic experiments," *Adsorption*, vol. 27, pp. 295–318, 2021.

[75] A. A. C. d. Santos, "Desenvolvimento de novas estruturas orgânicas metálicas (mofs) e estruturas orgânicas covalentes (cofs) para a remoção de poluentes ambientais tóxicos," Ph.D. dissertation, ISEL - Instituto Superior de Engenharia de Lisboa, 2022.

[76] E. Glueckauf, *Theory of chromatography.* J. Chromatogr. Libr., 1955, vol. 51.

[77] K. Y. Foo and B. H. Hameed, "Insights into the modeling of adsorption isotherm systems," *Chemical engineering journal*, vol. 156, no. 1, pp. 2–10, 2010.

[78] R. M. Barrer, "Zeolites and clay minerals as sorbents and molecular sieves," 1978.

[79] D. M. Ruthven, *Principles of adsorption and adsorption processes.* John Wiley & Sons, 1984.

[80] A. Henrique, A. E. Rodrigues, and J. A. Silva, "Separation of hexane isomers in zif-8 by fixed bed adsorption," *Industrial & Engineering Chemistry Research*, vol. 58, no. 1, pp. 378–394, 2018.

[81] L. F. Zafanelli, A. Henrique, M. Karimi, A. E. Rodrigues, and J. A. Silva, "Single- and multicomponent fixed bed adsorption of co2, ch4, and n2 in binder-free beads of 4a zeolite," *Industrial & Engineering Chemistry Research*, vol. 59, no. 30, pp. 13 724–13 734, 2020.

[82] E. Aly *et al.*, "Fixed bed adsorption of co2, ch4, and n2 and their mixtures in potassium-exchanged binder-free beads of y zeolite," *Industrial & Engineering Chemistry Research*, vol. 60, no. 42, pp. 15 236–15 247, 2021.

[83] M. Karimi, A. Ferreira, A. E. Rodrigues, F. Nouar, C. Serre, and J. A. Silva, "Mil-160 (al) as a candidate for biogas upgrading and co2 capture by adsorption processes," *Industrial & Engineering Chemistry Research*, vol. 62, no. 12, pp. 5216–5229, 2023.

[84] A. Bakhtyari and M. Mofarahi, "Pure and binary adsorption equilibria of methane and nitrogen on zeolite 5a," *Journal of Chemical & Engineering Data*, vol. 59, no. 3, pp. 626–639, 2014.

[85] D. Do, *Adsorption Analysis: Equilibria and Kinetics*. Imperial College Press, London, Jan. 1998, vol. 2, ISBN: 9781860943829. DOI: 10.1142/9781860943829.

Appendix A

Original Project Proposal

INSTITUTO POLITÉCNICO DE BRAGANÇA

Proposals for Dissertation/Project - Final Degree Project

Supervisor of the host Institution:

José A. C. Silva	jsilva@ipb.pt

Institution of the supervisor:

IPB	ESTiG

Co-supervisor of the partner institution:

<nome do orientador>	<email do orientador>

Institution of the co-supervisor:

<nome da Instituição>	<nome da Escola/Campus>

Schedule:

Chemical Engineering

Project title:

Separation CH4/H2 in 3D printing porous carbon monoliths

Keywords:

Separation CH4/H2; 3D printing porous carbon monoliths; Adsorption processes

Objectives:

In this work a series of 3D printing porous carbon monoliths will be studied regarding their ability to separate mixtures CH4/H2 for green hydrogen (GH) production regarding the development of new adsorption separation processes.

Additional description:

A main challenge for using the existing natural gas network to distribute blended GH is to separate it from the mixture (H2/CH4) at the end use to increase the value of the GH. Currently, cyclic adsorption processes (pressure swing adsorption (PSA)) is the mature technology used to produce high purity H2 (>99.99%). However, this technology cannot be economically upgraded for feed gases different from:H2(>50%)/CH4(<50%). GH blended in natural gas pipelines will require PSA units to purify H2 in the mixture range H2(<20%)/CH4(> 80%) (also for safety reasons) which discard the existing available mature PSA technology. This is so because actual existing adsorbents preferential adsorb CH4 over H2 which is practically an inert in contact with such adsorbents (therefore very large PSA units will be needed to adsorb the large quantities of CH4 in the pipelines).

Methodology/Work-plan:

1)Experimental fixed bed studies with mixtures H2(<20%)/CH4(>80%) to evaluate 3D activated carbon monoliths performance;

2) Experimental determination of kinetics, equilibrium constants, selectivity and loading capacity of CH4 and H2 im the 3D printed-AC momoliths;

Necessary resources:

Experimental apparatus exhisting in CIMO-ESTig